OCDO--95010708

OHIO COAL RESEARCH CONSORTIUM

SUBCONTRACT AGREEMENT NO. OCRC/93-2.1

OCDO Grant No. CDO/R-87-2C/B

INVESTIGATION OF TRANSPORT PROCESS INVOLVED IN FGD

Final Report for the Period
September 1, 1993 to August 31, 1994

by

J. R. Kadambi
J.S. T'ien
C. Yurteri
V. Kadaba
M. Assar

Case Western Reserve University, Cleveland, OH

February 1995

Project Manager: J.R. Kadambi, Professor, Mechanical & Aerospace Engineering,
Case Western Reserve University, Cleveland, OH 45221
(216) 368-6456

This project was funded in part by the Ohio Coal Development Office, Department of Development, State of Ohio.

TABLE OF CONTENTS

EXECUTIVE SUMMARY

This report describes the work done in the fourth year of the project " Investigation of Transport Processes Involved in FGD".The objectives of this five year plan of study are to experimentally obtain a basic understanding of (1) turbulent flow structure of the mixing zone and its influence on particle dispersion, (2) the effect of particle loading on turbulent properties and mixing, (3) the effect of jet entrainment, (4) water spray-sorbent interaction, sorbent wetting and mixing, (5) investigate the flow field where certain ratios of jet velocity to flue gas velocity result in regions of negative flow and define onset of negative flow , and (6) sorbent reactivity in immediate mixing zone.

In the first two years of the project a sorbent injection facility which can simulate the conditions encountered in COOLSIDE set up was designed and built. Non-intrusive laser based diagnostic tools PDA/LDA were used for flow characterization of particle laden jet in cocurrent flows . In the third year a new technique called TTLDV which combines particle transit time in measurement volume of LDV and LDV velocity measurements to simultaneously obtain non-spherical lime particle size and velocity was developed. Better sorbent injection schemes were investigated .Spray cocurrent flow tests were conducted.

During the fourth year the spray cocurrent flow interaction data was analyzed. A criterion was developed for predicting the flow reversal which results in deposition of water droplets on the duct wall (Table 3). The flow reversal occurs when the spray has entrained all the cocurrent flowing stream . The criterion is based upon the mass flow rate of the two phases . The criterion successfully predicted the flow reversals encountered in the experiments and will be a very useful

practical tool.

Lime laden jet cocurrent flow interactions tests were completed . Tests on the swirling nozzle have been conducted. The single phase data have been analyzed while the two phase glass particle laden jet data is being analyzed . Based upon the analyses of the results ,the swirl plate axial length , height and twist angle can be varied . No extra energy is required to enhance the mixing . The results indicate that the mixing is enhanced and the turbulence intensities in the radial direction show an increase of 10 to 30 %.

Tests indicate that the spray droplet size obtained from SS 1/8 JJ nozzle are the proper size for studying particle water droplet interactions . Initial tests with water and glass bead slurry to ascertain the capacity of the multiphase software to differentiate between water droplet , glass particles and water coated glass particles indicate that the technique can be used . However to obtain cocurrent air flow at temperatures of 160 degree F as suggested by the project monitor to simulate the flue gas temperature , a heating system was ordered . The heating system is being installed .

The equipment needed for modification of the facility to simulate sulfur dioxide laden flue gas and for removal of the sulfur dioxide prior to releasing the simulated flue gas was investigated. Safety concerns raised by the environmental safety department implied a substantial and costly modification of the facility. This was brought up during the July OCRC meeting and it was suggested that the spray dryer facility at University of Cincinnati (PI Dr. T. Keener) may be utilized for this purpose. The PI and the graduate student visited Dr. Keener's laboratory .It was decided that sulfur dioxide tests will be carried out

at the spray dryer facility . A test set up to fit in the spray dryer facility conveniently has been designed.

Satisfactory progress has been made in the project during the fourth year . However , the PI , Dr. J.R. Kadambi underwent open heart surgery in April 1994 and that had some effect on the project . The PI has recovered from the surgery and is deeply involved with the project . Inspite of this setback all the tasks associated with the fourth year, were addressed.

One of the graduate students , Mr. V.P. Kadaba successfully defended his M.S. thesis and graduated in May , 1994.

Publications:

The following publications and presentations resulted from the fourth year work.

1." A New Approach Using Transit Time for Simultaneous Measurement of Size and Velocity of Non-spherical Particles," C.Yurteri, V.Kadaba and J.R. Kadambi,Laser Anemometry : Advances and Applications , ASME Symposium. FED vol 190, June,1994.

2. " Spray Cocurrent flow Interactions and Flow Reversal," V.Kadaba, C.Yurteri and J.R. Kadambi, accepted for ASME Solid -Liquid Flow Symposium to be held at Hilton Head, August, 1995.

3." A Simultaneous Measurement of Irregular Particle Size and Velocity using Transit Time and LDV," M.Assar, C.Yurteri,V.Kadaba and J.R.Kadambi . Flow Instrumentation Forum, FED vol. 161, ASME , New York,NY . 1993.

A poster session presentation of the TTLDV work was also made at NASA Lewis research Center sponsored Advanced Subsonic Transport Workshop held at Cleveland , Ohio in August 1994.

1. INTRODUCTION

Complicated multiphase flows (solid-gas, gas-liquid-solid and liquid-gas) are involved in many FGD processes. Multiphase flows by themselves are not well understood and their impact on FGD processes are even less understood. Drummond et al.(1) in their discussion of duct injection technologies for SO_2 control have included the transport and chemical processes within the duct, fluid mechanics of the system, nozzle design and operation, and humidification system designs areas of concern which require research to develop a better understanding of the process. The improvements in the basic knowledge of fluid mechanics, heat and mass transfer rate effects are needed (Reference 2) to understand and achieve substantial improvements in many key areas of FGD processes and obtain scale-up criteria. Dry sorbent injection and dispersion, sorbent humidification by water injection, sorbent slurry injection, material handling aspects of sorbent slurry, sorbent powder and ash are some examples. In the utilization of high-sulfur Ohio coal emphasis has been placed on increasing the efficiency of dry, high sulfur flue gas scrubbing processes using calcium-based sorbents (LIMB, COOLSIDE). This entails the need to improve our understanding of the mixing processes which play a crucial role in enhancing sorbent utilization.

The reaction between SO_2 and sorbent particles involves mixing resulting from gross flow patterns and turbulence, mass transfer due to diffusion and dispersion and finally chemical reaction. Since the sorbent particles are injected into the flue gas, a prerequisite for fast reaction is the rapid mixing of the sorbent particle from the

injection nozzle with the flue gas stream. Free jet entrainment might probably be a very important mechanism of rapid mixing. Clearly mixing is determined by flow patterns and turbulent flow processes which are influenced by the characteristics of the injection jet and interactions with the surrounding stream. Additionally, the wetting of sorbent particles with water spray seems to improve the sorbent utilization. The literature review reported in the first year work Kadambi et al (3) indicated that the experimental data available in the area of induct flue gas desulfurization process (FGD) is sparse and does not cover the range of interest of dry FGD processes. So far, many of the fundamental questions involved in solid-gas and solid-liquid-gas flows have not resolved. In addition, the mixing of the sorbent particles in FGD processes can possess different features because of different particle size, jet Reynolds number, particle loading and agglomeration properties.

The particle-laden flows are inherently more complex than the single phase flows. This follows from the fact that the particles are distinct from the fluid, the continuous phase element. First, unlike the fluid element, the particles have finite size and shape and cannot deform under strain. Viscous forces result when particle surface velocity is different than the velocity of the surrounding fluid. Secondly, there is usually a substantial density difference between solids and the continuous gas phase. Thus, these particles have much more inertia than the fluid elements moving out at similar velocities and are, therefore, unable to follow every scale of fluctuation of the fluid flow. In case of mismatch between the fluid and particle

velocities, the particles exchange energy and momentum with the fluid through viscous drag. Faster moving particles might increase local fluid velocities by dragging along the fluid and vice versa. Particles may dampen or amplify the fluid fluctuation levels in different scales of eddies as a result of this interaction. A sufficiently large particle mass loading can result in the modification of the overall turbulence levels. For high particle loading, interaction among particles and the interaction of particles wakes can further complicate the flow.

The inertia of a particle in fluid flow can be assessed quantitatively by calculating a particle time constant. Assuming Stokesian flow, and that the particle density is substantially larger than fluid density, the time t_p taken for the particle to accelerate from rest to 63% of the free stream velocity is given by

$$t_p = \rho_p d_p^2 / 18 \mu$$

where

ρ_p = particle density

d_p = particle diameter

μ = fluid viscosity.

A fluid time scale t_f based upon a given eddy can be given by

$$t_f = L/U$$

where

L = eddy length scale

$\acute{U}$ = eddy velocity scale.

Based upon relating t_p and t_f, the particle and fluid time scales, we can divide the possibilities of particle responses to turbulent flow into three regimes. In the first regime, if $t_p >> t_f$, a particle will not respond to fluctuations in the flow. For example, paths of heavy large steel balls dropping through air will not be affected by turbulent eddies. In the second regime, if $t_p << t_f$, a particle will completely follow the flow including any fluctuations. The seed particles used in Laser Doppler Anemometry (LDA) measurements to obtain flow velocities are assumed to behave in such a manner. The third possible regime occurs when both t_p and t_f are of the same order of magnitude. In such a case particles respond partially to the fluctuations in the flow. Here, the particles are not able to follow the fluid elements exactly, but their paths are altered by fluid fluctuations. The flow in this regime is most poorly understood and is very difficult to model. This regime may also encompass the induct injection processes. The injection of the particle-laden jet into cocurrent flow further complicates the process. The wetting of the sorbent particles with water spray appears to enhance sorbent utilization. This makes the flow solid-liquid-gas multiphase flow with all the associated complexities. A review of literature was undertaken in this area of spray cocurrent flow and was reported by Kadambi et. al (3,5). No paper in the area of interaction

of water spray and particles in cocurrent flow relevant to dry FGD processes was obtained. The following conclusions were drawn from the review.

Though there have been some studies of two phase mixing problems and particle laden jets, so far, many of the fundamental questions involved in the two and three phase flows, especially relevant to FGD processes, have not been resolved. In addition, the mixing of the sorbent particles in FGD processes can possess different features because of different particle sizes, jet Reynolds number, particle loading, and agglomeration properties. The information required to develop a better understanding of the phenomenon of mixing relevant to FGD processes where two or three phase, gas-solid, gas-solid-liquid, turbulent, horizontal jet issues into a cocurrent flow with relatively smaller diameter particles has to be developed.

Injection of fine spray of water into the duct appears to enhance the sorbent utilization. However, the residence time of the droplets (e.g. 30 micron diameter) is about 2.5 seconds to 3.0 seconds before evaporation, and the interaction between the water droplet has to take place before that. The interaction between the water droplet and sorbent has to be improved so as to enhance wetting and mixing. The scavenging has also to be improved. There is need for experimental data to validate, develop and improve water spray and two phase slurry models. The emphasis being on mixing, dispersion and increasing turbulence. Another issue of interest is the location of water spray and sorbent injection location relative to one another along the axial direction. Additionally, for certain ratios of spray velocity to flue

gas velocity regions of negative flow appear and there is a need to define onset of such negative flows to avoid such flow conditions in FGD process.

1.1 Five Year Plan Objectives :

A five year plan was developed to improve our understanding of such flows involved in dry FGD processes.

The objectives of this five year plan of study is to experimentally obtain a basic understanding of (1) turbulent flow structure of the mixing zone and its influence on particle dispersion, (2) the effect of particle loading on turbulent properties and mixing, (3) the effect of jet entrainment, (4) water spray-sorbent interaction, sorbent wetting and mixing, (5) investigate the flow field where certain ratios of jet velocity to flue gas velocity result in regions of negative flow and define onset of negative flow , and (6) sorbent reactivity in immediate mixing zone. Some of these objectives have been addressed in this investigation. The first three years work will be briefly discussed and then the results of the fourth year work will be presented.

2. PREVIOUS ACCOMPLISHMENTS

2.1. Work Accomplished in the First Two Years (9/90 - 8/92)

To properly simulate the conditions encountered in induct sorbent injection FGD process set ups, geometric, dynamic and kinematic similarity parameters the range of Reynolds number, Stokes number, Froude number, the particle laden jet to cocurrent stream momentum flux ratio and the mass loading ratio encountered in FGD processes were duplicated. This criteria was used in designing and building the test facility (Reference 3).

A 7.3 mm diameter tube is used for injecting the solid particle laden jet into a 88.6 mm by 88.6 mm square duct(Figure 1). The duct is made up of transparent plexiglass walls except for the 300 mm long test section which is made up of pyrex glass. The glass sides and the square configuration of the duct facilitates the use of laser based non-intrusive Particle Dynamics Analyzer (PDA) for obtaining particle size and velocity simultaneously. The particle material used in the tests are glass, and lime particles in the size range of 5 to 100 micrometer diameter. The glass particles are spherical while the lime particles are not spherical. Since the PDA performance depends upon the particle sphericity, in the first series of tests (in the second year) spherical glass particles were used. To ensure proper mixing of the particles and the jet air stream, the particles were added at a location far upstream (x/d=100) of the particle laden jet exit into the duct. The particle laden flow is then led into the 7.3 mm diameter jet tube. A range of mass loading (0 to 10) was obtained. The interaction between the particle laden jet and cocurrent duct flow occurs in the test section.

Details of the sorbent injection test facility are provided in Reference 3.

The major instrumentation used is the Particle Dynamics Analyzer (PDA). The PDA manufactured by Dantec Electronics utilizes a 4 watt Argon-ion laser. The PDA simultaneously measures the size, velocity and concentration of the spherical particles. It is based upon Laser Doppler Anemometry and Phase Doppler Interferometry.

The details and principle of operation of PDA/LDA are provided in Reference 4 (DANTEC Manual).

The uncertainties in the measurements were as follows. For PDA/LDA measurements: Traverse accuracy ± 0.01 mm, Velocity measurements ± 1.5%, Particle diameter ± 8%, and concentration ± 4%. For turbine flowmeter ± 1%, Flowrator ± 2%, and particle mass loading ± 1.0% The test details are provided in our second year report (Reference 3). Some important conclusions from the first 2 years were:

- Phase Doppler Anemometry was successfully utilized for studying particle-laden flows. Particle size and velocity and flow velocities were obtained allowing us to discriminate between the phases.
- The particle velocities were less than the single phase fluid velocities along the centerline near the exit of the jet. At downstream locations greater than x/d = 10 the situation reversed with the particle velocities being greater than the fluid velocities, since, the axial velocity decay is faster for single phase than that for particle phase due to higher spreading of shear layer in single phase. This phenomenon is further enhanced

with the increase in particle loading due to inertia.

- The slip velocity was nearly constant for all mass loadings.
- Addition of the particles to the flow resulted in an increase in the gas-phase mean velocities.
- Particle mass loading has a significant effect on the development of the particle laden jet. These include the following. (a) In the radial direction along the width the particle mean velocities and the fluctuating components are dependent upon the mass loading. Larger mass loading results in higher mean velocity and smaller fluctuating component, (b) the presence of particles was found to suppress turbulent fluctuations, since Re_p=O(1). This is also known as turbulence modulation and results in the reduction in the turbulence intensity and shear stress. These effects became more pronounced when mass loading was increased, and (c) Jet spreading rate decreases with increasing mass loading, which results from the reduction in the radial fluctuation velocity.
- It was found that particle laden jet entrainment depends upon the jet velocity, mass loading, and axial distance. Entrainment increase with higher jet velocity and lower mass loading.
- Since, the higher mass loading results in a lesser spreading rate, the particles are concentrated in a smaller radial distance and there is a resulting reduction in the particle dispersion and mixing.
- Mass loadings greater than 5, result in the reduction in turbulence intensity, Reynolds stress, jet entrainment and spreading rate. That is, the mixing is reduced. Lower mass loadings, m<5, show

better mixing characteristics and therefore may be beneficial for induct injection processes.

2.2 Work Accomplished in third year (9-92 to 8-93)

The third year tasks involved (a) conducting tests with lime laden jet flow ,(COOLSIDE Configuration), (b) Investigation of spray to cocurrent flow velocity ratio ranges and which result in region of negative flow, (c) investigate better sorbent injection schemes and (d) develop techniques to study particulate droplet interaction.

(a) TTLDV Technique:

The PDA technique can obtain simultaneous measurement of particle velocity and size for spherical particles (droplets) only. Lime particles are not spherical and therefore, PDA could not be used for irregular shaped lime particles. We therefore concentrated upon developing a technique 'TTLDV' for simultaneous measured of lime particle size and velocity. The TTLDV technique is based upon the measurement of the transit time of the irregular shaped particle to cross the known size of the measurement volume formed by the crossing of the two laser beams of the Laser Doppler Velocimeter (LDV), and the particle velocity obtained by LDV. The applicability of the TTLDV technique was ascertained by (a) using known size spherical glass beads and comparing PDA and TTLDV data as shown in Figure 2 and (b) using known size lime particles and comparing the TTLDV results with the known sizes. The lime particle size was obtained independently using Microtrac which utilizes Franhoffer light scattering technique. The comparison of TTLDV, Microtrac and PDA results for lime tests are shown in Figures 3. As can be observed from the figure TTLDV and Microtrac

results compare favorably but the PDA results are off by a factor of 4. Details of the TTLDV technique are provided in Reference 5 and 6.

(b) Investigation of spray - cocurrent flow interactions.

Flow reversal resulting from spray jet cocurrent flow interaction was investigated. Again, non-intrusive PDA/LDV technique were used for measuring the droplet velocity and diameter. SS 1/8 JJ atomizing nozzle was used. It was installed into the sorbent injection facility in the place of the particle laden jet tube in the 88 mm x 88mm duct. The characteristics of the atomizing nozzle were obtained. The complete test data included 36 sets (about 144 axial locations). The test data analyzes was started near the end of third year and was completed in the early part of fourth year. The data analyzes will be discussed in the section dealing with the fourth year work.

(c) Swirling co-flow atomizer (injector) was selected for obtaining better mixing of the droplets with the cocurrent flowing air. The swirl atomizers requires relatively simple arrangement of swirl plates, without additional energy requirements.

(d) A multiphase data acquisition program which was acquired and was used to investigate droplet-glass particle interaction felt that this technique TTLDV technique may be useful in the droplet-particle interactions.

The highlights of 1993 work included.

· Development of TTLDV Technique for simultaneously measurements of irregular shape particle size and velocity. The TTLDV provides a very useful tool for solid-fluid multiphase flows. It was used for studying lime laden flows.

· Completion of tests to investigate spray-cocurrent flow interactions. SS 1/8 JJ nozzle was used.

· Swirl co-flow atomizer was selected as the geometry for tests to investigate/obtain more efficient sorbent injectors.

3. WORK PERFORMED IN THE FOURTH YEAR (1994-95)

The fourth year tasks included:

(1) Completion of spray cocurrent flow interaction and development of criterion to predict flow reversal, (2) Continue tests on new nozzle configuration (initiated in the third year), (3) Evaluate optimum manner of injecting hydrated lime into cocurrent flow (i.e. flue gas) to improve sorbent utilization (4) Conduct tests to obtain flow configuration (nozzle/spray atomizer) to maximize inelastic collision between water droplet and sorbent), (5) Test the configuration of (4) for mixing characteristics and (6) Plan and modify sorbent injection test facility to obtain simulated flue gas with SO_2.

The following has been accomplished in the fourth year.

3.1 Results of Spray-Cocurrent Flow Interaction Investigation (Task #1)

The sorbent injection test facility (Figure 1) was used for these tests. Table 1 provides the test facility specifications. The SS 1/8 JJ atomizing nozzle from Spraying Systems Inc. was mounted in the center of the 88.6 mm by 88.6 mm square duct. This nozzle was chosen for its similarity to those sprays encountered in flue gas desulfurization (FGD) processes applicable to this study. The nozzle inner diameter is 1.3 mm. The spray atomizer is mounted as close as possible to the test section. A honeycomb is placed at the upstream end of the duct to

insure uniform flow for the cocurrent air flow (gas phase).

The atomizing nozzle consists of a mixing chamber in which pressurized air and water are mixed to produce the spray. Air to the atomizing nozzle is regulated using a pressure gauge. The water is obtained from a constant pressure tank and the flow rate is measured using a water flow meter just upstream of the atomizer entrance. The atomizer was carefully aligned to insure that the spray exit is parallel to the duct walls.

Test conditions are shown in Table 2. Tests were conducted for given spray conditions and cocurrent air flow rates. Measurements were made at four specific axial locations. Velocity, spray droplet size, and concentration measurements were made at axial locations of 5, 10, 20, and 30 cm for each test. The test section window (optical view port) allows for the use of laser based non-intrusive measurement techniques (PDA/LDA). The air temperature and water temperatures were measured at inlet to the atomizer and the duct. The water from the liquid phase is gathered at the end of the duct by a cyclone separator. The ranges of the flow instrumentation and their accuracy levels are described in Appendix-A. Preliminary tests were conducted to determine if the spray is indeed axisymmetric. The probe (measurement) volume was placed at the top center of the duct at an axial distance of 10 cm from the nozzle exit. The air pressure of the nozzle was 60 psig (0.414 MPa) and the water flow rate was 50 cc/min. The spray was traversed downward over the entire length of the duct and measurements were made in the x-y plane. This procedure was repeated starting from the back center of the wall, at an axial distance of 10 cm, and traversing the spray forward.

This constitutes measurements in the x-z plane (Figure 4(b). The velocity profiles in the two planes match very well (Figure 4). The test was repeated at an axial location of 20 cm from the nozzle exit. Again the velocity profiles are virtually identical. Thus, the spray is shown to be axisymmetric.

Once axisymmetry of the spray is established, it is only necessary to traverse half the duct and in one single plane. Each experiment begins at a fixed water flow rate and atomizer air pressure. The cocurrent air is set at 10 m/s, so that the duct Reynolds number will be similar to the Reynolds number in FGD processes, and the spray is traversed at four axial locations: 5, 10, 20, and 30 cm from the nozzle exit. The probe is then returned to the 5 cm axial location and the cocurrent air velocity is reduced. Again measurements are taken at the four axial locations. The cocurrent air velocity is then decreased again until the reversal of flow becomes obvious. This reversal is accompanied by the wetting of the test section window. Once reversal takes place, it is impossible for the laser beam to penetrate the test section window and no further measurements are possible. The experiment is stopped and the test section is removed and cleaned. The next set of data is taken at a nozzle air pressure reduced by 10 psig. The entire process described above is then repeated. These experiments were performed for three different water flow rates.

The instrument used in obtaining velocity, particle size, and concentration measurements in this study is the Particle Dynamics Analyzer (PDA). The PDA is manufactured by Dantec Electronics and utilizes a 5 watt Argon-ion laser. This apparatus is equipped with

fiber transmission optics, receiving optics, and a model #58N10 signal processor. The PDA, which is based on Laser Doppler Anemometry (LDA) and Phase Doppler Interferometry, simultaneously measures the velocity, size, and concentration of spherical droplets and spherical particles (Reference 4).

The transmitting and receiving optics of the PDA were mounted on a three dimensional traverse allowing for the mapping of the spray in the entire duct. Measurements were taken in back scatter second order refraction mode at an angle of 152 degrees, as suggested by Dantec's instruction manual based on the refractive index of water. Each measurement data set consisted of 4000 PDA/LDA measurements.

The PDA allows for the simultaneous measurement of velocity, particle size, and concentration of spherical particles or droplets. This technique cannot be relied upon for measurements of non-spherical particles. Due to surface tension, most of the water droplets issuing from the nozzle are of spherical form. However, at the 5 cm location, the PDA was not able to validate approximately twenty percent of the droplets due to a lack of sphericity.

3.2 Discussion of Experimental Results

The first stage of the experiment justified the assumption of spray axisymmetry. A series of tests were conducted to measure spray velocities and particle diameters using the PDA for different flow conditions (Table 2). Results of these tests are discussed in the following sections. At several test conditions reversal of the spray became obvious. A detailed discussion of flow reversal and a criterion defining it's onset is provided in this section.

3.2.1 Mass Balance

In order to verify the accuracy of the PDA/LDA results, a mass balance was performed at the 5 cm axial location. The amount of mass flow exiting the nozzle was calculated by integrating over the velocity profile inside the spray envelope at the 5 cm axial location. When compared with the known mass flow entering the atomizer, the agreement is within six percent. This small amount of ambiguity is attributed to the evaporation of water droplets.

3.2.2 Spray Axisymmetry

The objective for establishing the axisymmetric characteristics of the spray was to ensure that the flow field was identical in all planes through the centerline. An additional advantage is that it facilitates measurements of the spray characteristics. The existence of axisymmetry permits measurements to be made for half the duct. The atomizer water flow rate in this experiment was set at 50 cc/min and the air pressure in the atomizer was measured at 60 psig (0.414 MPa). The cocurrent air speed in the duct was 10 m/s. Measurements were made at 1 mm intervals traversing the duct in both the x-y and x-z planes (Figure 4b). The experiment was conducted at 10 (x/d_0=76.9), and 20 cm (x/d_0=153.8) axial distances downstream of the nozzle exit. Each measurement consisted of 4000 PDA/LDA measurements.

The data obtained from these measurements were plotted at each axial location. The velocity profiles for the two planes are nearly identical and are shown in Figure 4. Only very close to the wall do the curves not match exactly and this slight mismatch is attributed to low

3.3.3 Velocity Characteristics

Tests were run at various nozzle air and water flow rates as well as various cocurrent or duct air flow rates (Table 2). Each test started at a specific water flow rate, atomizer air pressure, and duct air flow rate. The cocurrent air speeds or duct flow rates were chosen so that the Reynolds number for the flow in the test section would be of the same order as the Reynolds number encountered in FGD processes. Due to axisymmetry one half of the duct was traversed in the radial direction. For these conditions the nozzle air and water flow rates are kept constant while varying the duct air flow rate from it's maximum value. This air flow rate is obtained from a turbine flow meter substantially upstream of the duct entrance. The majority of the tests were conducted at four different duct air flow rates; however, in several instances the test section wall became covered with water prior to the completion of the tests (i.e. covering the two furthest downstream axial locations) at the third duct air flow rate preventing measurements to be made using the PDA. This difficulty is due to reversal of the spray and will be addressed later in this chapter. The nozzle air pressure and water flow rates are obtained from a pressure gauge and flow meter, respectively. In addition, the atomizer air flow rate is measured using a flow meter. Careful attention was paid to ensure that the air pressure and water flow rate were held constant while the duct air flow rate was varied at pre-selected intervals for each set of tests. The first sequence of tests were conducted at the four duct air flow rates and at the highest atomizer pressure. This pressure was lowered for the next sequence of experiments.

The atomizer velocity profile at the 5 cm axial location displayed a similar curvature at every flow condition tested. Further downstream the velocity profiles began to flatten out with the centerline velocity decreasing significantly. At the 30 cm axial location the velocity profile is virtually flat for all test conditions. This situation is due to the dispersion of momentum as the spray expands

downstream. Figures 5-13 show representative velocity profiles for various conditions. In these figures, the velocity is normalized as,

$$\frac{U_s - u}{U_c - u}$$

where u_s is the measured spray velocity, u is the cocurrent air stream velocity and u_c is the measured centerline velocity at the 5 cm location. The maximum velocity for each case always occurs at the centerline. A model based on experimental data was developed to describe the velocity profiles inside the spray envelope. This model is based on the cosine function and is given by

$$\frac{u_s - u}{u_c - u} = \frac{1}{2}\{1 + \cos\frac{\pi r}{2y_{0.5}}\}.$$

A comparison of the experimental velocity profiles and the cosine model is shown in Figures 14-19. The PDA/LDA measurements taken at the 5 cm location were restricted to a smaller core part of the duct when compared to the downstream locations. This is explained by the fact that the spray had not expanded covering the entire duct since the measurement location is close to the atomizer.

Each velocity profile at the 5 cm axial location shows a linear decay from the second to the eleventh radial measurement location; after this radial location the profile begins to flatten rapidly. At the 10 cm axial location the velocity decay is linear from the third to fifteenth radial measurement location after which the profile begins to flatten. At the two furthest downstream locations the velocity profiles are flat near the centerline and then decay linearly at further radial locations all the way to the test section wall. It is noted that the slope of the linear velocity decay is virtually the same for the tests

conducted at constant atomizer flow conditions but varying cocurrent velocities at a given axial measurement location(Figures 20-26).

Velocity profiles plotted at the 5 cm location for fixed atomizer flow conditions and varying cocurrent air velocities are almost identical. The same is true for such plots at the 10 cm location with some variation near the wall due to low particle seeding (Figures 4.11-4.14). However, velocity profiles at the two furthest downstream axial locations do not exhibit this characteristic. Although, as stated above, the slope of the linear velocity decay is the same for velocity profiles at varying concurrent air flow rates, the velocity profiles are not identical (Figures 20-26). For higher cocurrent air flow rates at these downstream axial measurement locations greater velocities have been measured. The cocurrent air velocity decrease corresponds to the observed decrease in the velocity measurements at these downstream locations. The reason for this observed decay at the downstream locations and not at the upstream locations is related to the dominant momentum of the atomizer when compared to the momentum of the cocurrent flow in regions near the spray exit. The momentum of the spray is observed to be dispersed due to the expansion of the spray moving downstream. At the 20 cm location the momentum of the spray was observed to be significantly decreased and hence the jet no longer dominates the duct air flow. Rather, at the two downstream locations the cocurrent flow momentum has a significant influence on the spray velocity.

3.3.4 Non-dimensional Parameters

A non dimensional analysis was performed to reveal those parameters of importance in this experiment. The Reynolds number and the Euler number have been recognized to describe the experimental results as pertaining to the velocity characteristics of the flow. The Reynolds number is the parameter

representing the ratio of inertial forces to viscous forces in a given flow. The Reynolds numbers of the cocurrent air flow have been obtained using the average velocity of the duct air as measured using PDA/LDA

$$Re_a = \rho u_a d_a / \mu$$

Density and viscosity of air varied slightly with each test due to a slight change in air temperature. The range of air temperatures is shown in Table 2. This Reynolds numbers for these experiments ranges from 2.2×10^5 to 6.2×10^5.

The Reynolds number of the entire air flow was calculated for the experiment which includes the air issuing from the nozzle exit and the air flowing through the duct. This Reynolds number has been calculated by taking the ratio of the sum of the mass flow rates of the two air flows multiplied by the hydraulic diameter of the duct to the product of duct cross sectional area and air viscosity.

$$Re_a = (m + m_a) dh / A_c \mu$$

The incremental rise in Reynolds number is slight, but the values were similar to the Reynolds number of the cocurrent air mentioned before.

Velocity measurements were made at four different axial locations. At each location the spray was traversed in one millimeter increments from the centerline to the edge of the duct. The velocity decreased in a parabolic fashion as described above. In order to calculate a Reynolds number inside the spray envelope, the mean velocity at each axial measurement plane is used. The Reynolds number for the spray is defined as

$$Re_s = \rho u_m d_o / \mu$$

where d_o is the exit diameter of the nozzle. The values for this spray Reynolds number ranges from 400 to 4000.

3.4 Flow Reversal

As the cocurrent air flow rate in the duct is progressively reduced the emergence of flow reversal in the outer regions of the square duct becomes prominent. Such flow reversals are undesirable in flue gas desulfurization processes because this results in water droplets separating out from the flow onto the duct walls. Establishment of flow reversal will provide a basis to determine lower threshold values for the cocurrent flue gas flow in engineering applications. In other applications where atomizers are utilized, such as in rocket propulsion, the flow reversal will adversely affect the thermal performance. Flow reversal occurring downstream of the test section is not relevant to this study because in flue gas desulfurization processes a row of several atomizers are situated side by side and the flow from adjacent nozzles interact inhibiting flow reversal. The focus of this study is to avoid the reversal of flow in the region before the interaction of the various atomizers and the test section was designed with this in mind. In these experiments, as the cocurrent air flow rate is reduced, the flow reversal propagates all the way back to the nozzle spray location. As the test section wall became wet, preventing further measurements leading to the better understanding of the spray spread characteristics at the selected measurement planes, the experiments were terminated. This limitation is due to the fact that the water layer on the wall blocked the penetration of the two laser beams preventing the formation of the localized non-intrusive measurement volume at the desired locations within the duct.

Although flow reversal is visible to the naked eye, attempts were made to obtain the velocity profiles for those cases for which flow reversals were observed. The plots presented here do not show negative

velocity values. This limitation is attributed to the PDA which is capable of measuring the mean velocity of the spray and by the time the mean velocity is negative the duct wall is too wet, blocking the penetration of the laser beams, to make measurements at these locations. Each test was monitored closely and the data was recorded up to the point of flow reversal as observed by the naked eye.

Tests were conducted at three spray atomizer water flow rates of 50, 20, and 70 cc/min. At each water flow rate tests were performed for atomizer air pressures of 50, 40, and 30 psig. Additional tests were conducted at an atomizer air pressure of 20 psig and a water flow rate of 20 cc/min. This low atomizer air pressure was unattainable at the higher water flow rates because of the lack of the cocurrent air momentum in the nozzle at higher water flow rates which resulted in immediate wetting of the wall. For each water flow rate and atomizer air pressure, tests were performed at four different cocurrent duct air flow rates. These flow rates correspond to approximate gas phase (cocurrent air flow) velocities of 10, 8, 6, and 4 m/s. A matrix of test conditions is shown in Table 2. In several cases the test section wall was covered with water due to flow reversal preventing continuation of the experiments at the low cocurrent duct air speed settings.

Critical parameters at which flow reversal occurred are of great importance in this study and the engineering applications that are impacted by it. As mentioned above, experimental measurements were made at axial locations of 5, 10, 20, and 30 cm downstream of the spray nozzle. It is apparent that the presence of flow reversal is dependent on the amount of entrainment of cocurrent air by the atomizer spray. A ratio of centerline spray velocity at the 5 cm location to the cocurrent airflow velocity (Table 2. As this ratio is increased to a value of 20, the flow reversal at the downstream end of the test section is observed. Higher values of this ratio lead to more vigorous flow reversals affecting upstream growth as well as the spray exit. Tests run at ratio values less than 20 exhibited no flow reversal in the test

section.

A similar velocity ratio was calculated using the centerline velocity of the spray at the 10 cm location (Table 2). For this case, flow reversal was apparent at ratio values greater than 10. This drop in ratio is indicative of the spread characteristics of the cone, lowering the centerline velocity due to momentum dispersion. Again, at values much larger than 10 the flow reversal was more vigorous and grew upstream towards the spray atomizer. At values below 10, no flow reversal was present in the test section. Such extensive tests were not conducted at further axial locations and it was not possible to accumulate enough data to develop this ratio due to wetting of the wall caused by flow reversal. It is quite possible that this ratio of centerline spray velocity to cocurrent air flow velocity shows a linea r decay with respect to the onset of flow reversals for increasing downstream axial locations.

In order to develop a deeper understanding of the flow reversal phenomenon, a model for the velocity characteristics inside the spray region was obtained following the methods of Chigier and Be'er(8). The case they presented describes the flow characteristics for a gas jet in a coaxial stream of the same or different gas. They did not study two phase (droplet-gas) flow. The model was modified in order to better represent the test conditions encountered in this study.

It is evident that flow inside the spray envelope where the cocurrent air is being entrained is a function of the velocity ratio for the two streams as described above. Results are given in terms of the potential core, a region immediately downstream from the nozzle exit in which the velocity of the nozzle fluid remains unchanged. The potential core length, x_p, is obtained from

$$\frac{x_p}{d_0} = 4 + 55\lambda \qquad (1)$$

where l is the ratio of gas phase mass flow rate to liquid phase mass flow rate and is defined as

$$\lambda = \frac{\rho u}{\rho_0 u_0} \tag{2}$$

The denominator in this expression corresponds to the region just outside the nozzle exit. U_o is the velocity of the nozzle at the exit and P_o is the density of the mixture of air and water in the nozzle calculated using the relative mass fractions of air and water in the nozzle. Equation 1, similar to Chigier and Be'er's model, has been modified to fit the two-phase droplet-air experimental results. Based on this, the velocity decay on the centerline in the fully developed region is given by

$$\frac{u_c - u}{u_0 - u} = \frac{x_p}{x} \tag{3}$$

where u_c is the centerline velocity at a given axial distance x. Experiments were performed at four different axial locations and exhibit a decay of centerline velocity that is similar to the above expression. The rate of jet expansion can be shown as

$$\frac{y_{0.5}}{d_0 / 2} = \left(\frac{x}{x_p}\right)^{(1-\lambda)} \tag{4}$$

where y0.5 is the radial position where the velocity is equal to

$$\frac{U_{min} + U_c}{2}$$

In order to describe the velocity profile, a simple cosine function was chosen. This expression is given by

$$\frac{u_s - u}{u_c - u} = \frac{1}{2}\{1 + \cos\frac{\pi r}{2y_{0.5}}\} \quad (5)$$

A comparison of this velocity profile and those obtained experimentally are shown in Figures 14-19 for several different test conditions. This approximation is very reliable in regions far downstream from the spray ($x/d_o > 80$). The velocity distributions in this region are very similar to those obtained experimentally. Some ambiguity arises for flow in the region close to the nozzle exit and is attributed to several reasons. Equation 5 describes the flow of a free jet in a cocurrent stream but it's functional dependence has been adapted to fit experimental data for a duct jet. For the free jet the cocurrent velocity remains constant as one moves downstream, however, for the ducted jet, as the spray expands more of the cocurrent air is entrained in the flow and the flow cross section provides less area for the air stream. Thus, the gas phase velocity for the experimental conditions is not constant. It is very important to note that the cosine distribution describes the jet velocity inside the spray envelope only. The largest amount of ambiguity when comparing experimental results in the upstream region is at the edge of the spray. The discrepancies in this region are largely due to the fact that the model assumes the spray boundary to be linear. In the ducted jet however, the spray boundary "swells" outward. The amount of swelling is dependent on the flow rate of the cocurrent air. As the boundary is approached, the model defines an exact point where the spray velocity reaches the gas phase velocity based on this linear assumption. Discrepancies arise when experimental measurements are made in this region. Since the spray boundary is curved outward the spray velocity reaches the gas phase velocity at a greater

radial distance than that proposed by the model. As one moves downstream the jet momentum is dispersed during expansion and the curved boundary approaches the linear approximation made by the cosine model.

A correction factor was sought in order to harmonize the results obtained from the cosine model an those obtained experimentally. Many different functions were attempted including products and powers of functions varying inversely with x and even exponential functions. The complexity of the variation in the two results made this very difficult. Correcting for ambiguities in some regions would shift data originally in agreement producing discrepancies. The experimental data often intertwines with the theoretical model (Figures 14-15). Deviation between the two curves was not uniform, sometimes positive and sometimes negative, making a reliable correction factor illusive.

3.4.1 Prediction of Flow Reversal Initiation and Recirculating Mass Flow Rate

The cosine model is in good general agreement with the flow inside the spray envelope. Based on these results we will follow the approach presented by Chigier and Be'er (8) to predict the point of flow reversal initiation and the mass flow rate of the reversed flow.

A good physical understanding of this problem reveals that as the spray expands downstream the air flow of the gas phase is entrained by the jet. The emergence of flow reversal is based on a critical point in the flow field. At this point all of the mass flow of the gas phase is entrained by the jet but the spray has more room to expand. In order for the spray to continue downstream a recirculation zone develops enhancing the spray mass flow. The critical point at which flow reversal occurs will be called 'N'. Figure 27 shows the development of the flow field for a case with flow reversal. This critical point is based on the assumption that the spray boundary is linear just as the cosine model for

velocity distribution. The mass flow rate inside the spray envelope during expansion can be shown as

$$\dot{m}_s = \int \rho u dA = \dot{m} + \dot{m}_0 \tag{6}$$

where m is the mass flow rate of the gas phase and m_0 is the total mass flow rate issuing from the nozzle. Again, the critical point is reached when the entire gas phase mass flow is entrained by the spray. Substituting the cosine model described above (equation 5) for the velocity in equation 6 gives

$$\dot{m}_s = \int \rho [u + \frac{u_c - u}{2} \cos \frac{\pi r}{2 y_{0.5}}] 2\pi r dr \tag{7}$$

describing the mass flow rate inside the spray. Defining the critical point for flow reversal as X_N in the axial direction, $y_{0.5}$ becomes

$$\frac{y_{0.5}}{d_0 / 2} = (\frac{X_N}{x_p})^{1-\lambda} \tag{8}$$

Solution of equations 6 and 7 (Chigier et. al., 8) result in the definition of the onset of flow reversal as

$$X_N = 6.25 \theta' L \tag{9}$$

where θ' is the modified Thring-Newby parameter (Chigier et. al., 1972) for ducted flows and 2L is the hydraulic diameter of the duct. The modified Thring-Newby parameter is given by

$$\theta' = \frac{\dot{m} + \dot{m}_0}{\dot{m}_0} \frac{d_0}{2L} \left(\frac{\rho_0}{\rho}\right)^{1/2} \tag{10}$$

The mass flow rate of reversed flow, m_r, is calculated from

$$\frac{\dot{m}_r}{\dot{m}_0 + \dot{m}} = \frac{0.47}{\theta'} - 0.5 \tag{11}$$

This expression is developed from the idea that flow reversal occurs when all the cocurrent air flow is entrained by the spray before flow reversal begins. Then for the spray to continue to propagate, it requires more entrainment which is supplied when the flow recirculates. Thus the entrained mass flow, m_e, becomes, $m_e = m + m_r$. These results can be applied to the tests conducted in our study. For the case when the mass flow rate of water entering the nozzle is 20 cc/min and the air pressure in the nozzle is 0.345 MPa and a gas phase speed of 10m/s, using equations 9 and 10 to calculate ' and X_N reveals that the onset of flow reversal will occur at an axial location of 21.4 cm downstream of the nozzle. Recall that these equations were based on the assumption of a linear spray boundary. Using similar triangles, the axial distance required for the spray to reach the duct wall, X_w, is calculated from

$$\frac{L}{X_w} = \frac{1}{4 + 55\lambda} \tag{12}$$

For the case discussed before this value is $X_w = 20.25$ cm implying that the spray will reach the duct wall prior to the critical point and the flow will not reverse. This is in agreement with observations under these test conditions. Choosing the same nozzle flow conditions but a gas phase velocity of 6m/s and repeating the above analysis describes the critical point as $X_N = 16.34$ cm. For this case, the spray-

wall interaction is predicted at an axial location, X_w, of 19.1 cm allowing for flow reversal. Experimental results show that flow reversal was indeed observed under these test conditions at an approximate axial location of 20 cm and from equation 11, the recirculating mass flow rate is calculated as 29.7% of the overall mass flow rate. This procedure establishes a criterion for the determination of the onset of flow reversal. This criterion correctly predicted flow reversal for all test conditions at which flow reversal was observed. Table 4 shows a comparison of the flow reversal criterion with the experimental data. A step-by-step procedure of establishing whether flow reversal occurs or not is shown in Table 3. Table 5 shows the range of mass flow of recirculation for those tests in which flow reversal did occur.

3.5 Particle Sizing

Figures 28-32 shows that droplet diameter increases as distance from the centerline increases. Larger particles tend to move to the edge of the spray while smaller droplets remain at the centerline. These results are in agreement with Samuelson et al.

It was observed that with an increase in axial distance from the nozzle the mean droplet grew in size. This observation was also evident along the centerline location but at a slower growth rate. This is largely due to evaporation of smaller particles. As the momentum of the spray decreases at further downstream locations, the mass transfer between the spray and cocurrent air also increases. This leads to increased evaporation of smaller particles. In flue gas desulfurization processes, the cocurrent air will be at much higher temperatures leading to more pronounced evaporation effects.

3.6 Conclusions

The following conclusions are based on the results of this study.

- The spray is axisymmetric.
- Velocity profiles displayed similar curvature at the two closest measurement planes to the jet exit and were nearly flat at the two downstream locations. This was due largely to the dispersion of momentum inside the spray envelope.
- A cosine model was developed to predict the velocity profiles. The agreement between the model and the experimental results in regions of $x/d_0 > 80$ is within 5%.
- An equation for centerline velocity decay was developed and the agreement with experimental results is within 3%.
- The liquid phase flow characteristics were affected by the entrainment of the gas phase much more in regions downstream of the nozzle exit ($x/d_0 > 100$).
- The onset of flow reversal is predicted by the mass flow rates of the two phases. Flow reversal is defined as the negative flow arising beyond the point where all the cocurrent air mass flow is entrained by the spray. A criterion for predicting the onset of flow reversal was developed. This criterion successfully predicted flow reversal for all test conditions in which flow reversal was observed. The procedure to determine the existence of flow reversal is outlined in Table 3.
- A relation is developed which predicts the ratio of recirculating mass flow to total mass flow for flow reversal conditions.

Further details of the experimental and numerical investigations are provided in V. Kadaba's thesis(Reference 7).

3.7 Task # 2 and 3.

The lime laden tests with the edgewater nozzle configuration were completed. The next phase included tests on the new swirling nozzle configuration. The swirling nozzle is shown in figure 33. The length 'l' and height 'h' and the twist angle can be varied. The design allows the cocurrent flow to be swirled so as to enhance the mixing of the cocurrent flow with the particle laden jet. There is no need to spend any extra energy to enhance the mixing. Tests with single phase, i.e. air - air tests and two phase, i.e. particle laden jet - cocurrent flow tests were also completed. Figure 34 shows the swirling nozzle position in the test setup and the LDA beam locations.

PDA (Particle Dynamics Analyzer) and LDA(Laser Doppler Anemometer) were utilized to characterize the flow. Axial, radial mean velocities and the turbulent fluctuating components were obtained. The measurements have been made at x/d (axial location downstream of nozzle/nozzle orifice diameter) equal to 0.2.,5,10,15 and 20 for the single phase tests. The number of measurements at each measurement location were varied between 500 to 5000. The single phase data have been compared with the Coolside configuration (which is a straight tube). Initial data analysis indicates that the flow emanating from the swirling nozzle has higher fluctuating components (turbulent intensities) of velocity in the radial as well as the axial direction as compared to the Coolside configuration. An increase of more than 15% is observed in the fluctuating components of the axial velocity. The increase in the fluctuating component of the radial velocity is greater than 10%. The level of increase is dependent upon the axial location and generally increases as one moves away from the nozzle. Increase in turbulent intensities, especially in the radial direction, implies better diffusion and consequently better mixing rates. Figure 35 shows the velocity map for the single phase jet mixing in cocurrent flow, indicating good mixing 20 diameters downstream of the nozzle. Figures 36,37 show some of the results

which indicate enhanced turbulent intensities in the radial and axial directions. The two phases. i.e. particle laden jet data for the swirling flow is being analyzed.

3.8 Task #4

Task 4. The analysis of flow reversal tests indicate that the SS 1/8 JJ nozzle is the proper water atomizing nozzle for studying the collision between water droplets and particles. Preliminary tests were conducted with water and glass bead slurry using a siphon type atomizer to ascertain the capability of the multiphase software to differentiate between water droplets, glass particles and the water coated glass particles. The tests indicate that the technique can be used for the task.

3.9 Task #5 and 6

These tasks involved modifications in the test facility. We ordered heaters so that the cocurrent flow temperatures of about 160°F could be maintained for task 5. The heaters were received and are in the process of being installed.

For task #6, the equipment needed to simulate flue gas in the facility and to ensure removal of sulfurdioxide prior to releasing the simulated gas into laboratory environment was investigated. Some problems were encountered with safety concerns raised due to the presence of sulfur dioxide. The satisfactory solution of the safety concern. it appeared would require a substantial investment in the facility. This was brought up during the July presentation to OCRC. It was then suggested to look into the possibility of running this test in the Sprayer Dryer Test facility at University of Cincinnati, associated with Dr. T. Keener's project. The PI and the graduate student visited Dr. Keener's laboratory, and it was found that it would be convenient to conduct the tests there. The tests will be conducted in the spring of 1995 at a mutually convenient time slot. A setup for the swirling nozzle and simple nozzle arrangement in the Sprayer Dryer facility is shown in Figure 38. The arrangement goes

between the Spray Dryer and the Fabric Filter. There will be provision to obtain spent lime samples immediately upstream of the Fabric Filter. The lime sample will then be evaluated to assess its utilization. The set up is being manufactured.

4.SUMMARY AND STATUS

Satisfactory progress has been made in the project during the fourth year . However , the PI ,Dr. J.R. Kadambi underwent open heart surgery in April 1994 and that had some effect on the project . The PI has recovered from the surgery and is deeply involved with the project . Inspite of this setback all the tasks associated with the fourth year, as indicated in the preceding sections, were addressed.

The spray cocurrent flow interaction data was analyzed. A criterion was developed for predicting the flow reversal which results in deposition of water droplets on the duct wall (Table 3). The flow reversal occurs when the spray has entrained all the cocurrent flowing stream . The criterion is based upon the mass flow rate of the two phases . The criterion successfully predicted the flow reversals encountered in the experiments .

Lime laden jet cocurrent flow interactions tests were completed . Tests on the swirling nozzle have been conducted. The single phase data have been analyzed while the two phase glass particle laden jet data is being analyzed . Another configuration of the swirling nozzle will be evaluated . Based upon the analyses of the results ,the swirl plate axial length , height and twist angle can be varied . No extra energy is required to enhance the mixing . The results indicate that the mixing is enhanced and the turbulence intensities in the radial direction show an increase of 10 to 30 %.

Tests indicate that the spray droplet size obtained from SS 1/8 JJ nozzle are the proper size for studying particle water droplet interactions . Initial tests with water and glass bead slurry to ascertain the capacity of the multiphase software to differentiate between water droplet , glass particles and water

coated glass particles indicate that the technique can beused . However to obtain cocurrent air flow at temperatures of 160 degree F as suggested by the project monitor to simulate the flue gas temperature , a heating system was ordered . The heating sytem is being installed . The tests were planned after the completion of swirl nozzle optimization.

The equipment needed for modification of the facility to simulate sulfur dioxide laden flue gas and for removal of the sulfur dioxide prior to releasing the simulated flue gas was investigated. Safety concerns raised by the environmental safety department implied a substantial and costly modification of the facility. This was brought up during the July OCRC meeting and it was suggested that the spray dryer facility at University of Cincinnati (PI Dr. T. Keener) may be utilized for this purpose. The PI and the graduate student visited Dr. Keener's laboratory .It was decided that sulfur dioxide tests will be carried out at the spray dryer facilty during spring of 1995 at a mutually convinient time . A test set up to fit in the spray dryer facilty convineintly has been designed.

One of the graduate students , Mr. V.P. Kadaba successfully defended his M.S. thesis and graduated in May , 1994.

Publications:

The following publications and presentations resulted from the fourth year work.

1." A New Approach Using Transit Time for Simultaneous Measurement of Size and Velocity of Non-spherical Particles." C.Yurteri, V.Kadaba and J.R. Kadambi.Laser Anemometry : Advances and Applications , ASME Symposium. FED vol 190. June.1994.

2. " Spray Cocurrent flow Interactions and Flow Reversal." V.Kadaba, C.Yurteri and J.R. Kadambi, accepted for ASME Solid -Liquid Flow Symposium to be held at Hilton Head, August, 1995.

3." A Simultaneous Measurement of Irregular Particle Size and Velocity using Transit Time and LDV."

M.Assar, C.Yurteri,V.Kadaba and J.R.Kadambi . Flow Instrumentation Forum, FED vol. 161, ASME , New York,NY . 1993.

A poster session presentation of the TTLDV work was also made at NASA Lewis reasearch Center sponsored Advanced Subsonic Transport Workshop held at Cleveland , Ohio in August 1994.

5. LITERATURE REFERENCES

1. Drummond, C., Babu, M., et al., "Duct Injection Technologies for SO_2 Control", Proceedings of First Combined Flue Gas Desulfurization and Dry SO_2 Control Symposium, EPRI Report GS-6307, St. Louis, MO, Oct. 1988.

2. Adler, R.J. Fan L.S., Kadambi, J.R., Keener, T.C., Khang, S.J., Prudich, M., and Raghunathan,K., "Flue Gas Desulfurization and Acid Rain Control," Report of the Consortium of Ohio Universities to OCDO, Sept. 1989.

3. Kadambi, J.R., Chinnapalaniadi, P. and T'ien, J.S. "Investigation of Transport Processes Involved in FGD", Final Report for Second Year, for Period September, 1991 to August 1992, submitted to OCDO, November 1992.

4. Dantec Electronics Inc, "Particle Dynamics Analyzer," User's Manual.

5. Kadambi, J.R., Yurteri, C., Kadaba, V. and Assar, M., "Investigation of Transport Processes in FGD - Third Year Final Report (OCRC93-2.1), submitted to OCDO. September 1993.

6. Yurteri, C., Kadaba, V. and Kadambi, J.R., "A New Approach Using Transit Time for Simultaneous Measurement of Size and Velocity of Non-Spherical Particles," Laser Anemometry Applications Symposium, ASME Summer Fluids Engineering Meeting, Lake Tahoe, NV., June, 1994.

7. Kadaba, V.P., "Spray Characterization of a Nozzle in Cocurrent Flow", M.S. Thesis, Department of Mechanical Engineering, Case Western Reserve University, Cleveland, Ohio. May, 1994.

8. Chigier, N., and Beer, L.M., Combustion Aerodynamics, J. Wiley and Sons Inc., New York, NY. 1972.

9. Sameulson, S.G., McDonnell, V.G., "Application of Laser Interferometry to Study of Droplet/Gas Phase Interactions and Behavior in Liquid Spray Combustion Systems', Comb. Science and Tech., Vol 79, 1990.

6. NOMENCLATURE

A viscous force per unit volume

B momentum transfer rate per unit volume due to mass transfer

C_D drag coefficient over the droplets

d average diameter of water droplet

d_0 exit (orifice) diameter of nozzle

D interphase drag per unit volume

Eu_D Euler number for the gas phase

Eu_s Euler number for the liquid phase

F_D drag force over one droplet

g gravitational constant

k empirical coefficient

L_m nondimensional momentum equilibration length

$\dot{m}$ mass flow rate of the cocurrent air

$\dot{m}_a$ mass flow rate of the air in the nozzle

$\dot{m}_r$ mass flow rate of recirculation

$\dot{m}_0$ mass flow rate at nozzle exit

$\dot{m}_w$ mass flow rate of water in nozzle

M_L liquid volumetric flow rate through atomizer

n number of droplets per unit volume of fluid

P pressure of gas phase

$\bar{P}$ dimensionless pressure

P_0 pressure at nozzle exit

r radial direction

$\bar{r}$	dimensionless radial direction
r_s	distance from centerline to edge of spray
Re_a	Reynolds number for the gas phase and atomizer air
Re	Reynolds number for the gas phase
Re_s	Reynolds number for the liquid phase
t	time
T	temperature
u	velocity of gas phase in axial direction
$\bar{u}$	dimensionless velocity (axial component)
u_c	velocity at centerline of spray (5 cm from nozzle exit)
u_d	velocity of liquid phase in the axial direction
u_0	velocity at nozzle exit
u_s	spray velocity
v	velocity of gas phase in radial direction
$\bar{v}$	dimensionless velocity (radial component)
v_d	velocity of liquid phase in the radial direction
W	width of the duct
x	axial direction
$\bar{x}$	dimensionless axial direction
x_p	potential core length
X_N	axial location of flow reversal initiation
X_w	axial distance required for spray to hit wall
Z	dimensionless parameter
ρ	density of gas phase (air)
Γ	mass transfer per unit volume due to phase change

τ_m time droplet takes to adjust to cocurrent air stream

ρ_f density of water

μ dynamic viscosity of air

μ_{eff} effective viscosity due to turbulence

ρ_d liquid phase density

β volume fraction of droplets in the mixture

θ direction in polar coordinate system

ν_{eff} effective kinematic viscosity due to turbulence

v_0 reference velocity in the radial direction

TABLE 1 TEST FACILITY PARAMETERS AND SPECIFICATIONS

Nozzle Orifice Diameter	1.3 mm
Outer Square Duct	88.6 x 88.6 mm^2
Test Section Length	300 mm
Cocurrent Air Velocity	4 - 11 m/s
Centerline Spray Velocity (5 cm)	50 - 110 m/s
Centerline Spray Velocity (10cm)	25 - 65 m/s
Temperature of Cocurrent Air	27 - 35 ^0C

Table 2 Test Conditions

Mass flow rate of water in atomizer, $\dot{m}_w$ (kg/s)	8.3×10^{-4}, 3.3×10^{-4}, 1.2×10^{-3}
Mass flow rate of air in atomizer, $\dot{m}_a$ (kg/s)	1.1×10^{-3}, 8.9×10^{-4} 7.2×10^{-4}, 5.7×10^{-4}
Axial Measurement Location (cm)	5, 10, 20, 30
Non-dimensional Measurement Locations (x/d_0)	38.5, 76.9, 153.8, 230.7
Air density, ρ (kg/m^3)	1.17
Water density, ρ_f (kg/m^3)	997.7

	Atomizer Conditions		Duct Air Flow Conditions
	Water Flow Rate(cc/min)	Air Pres.(psig)	Duct Air Flow (m/s)
Case 1:	50	50	10, 8, 6, 4
Case 2:	50	40	10, 8, 6, 4
Case 3:	50	30	10, 8, 6, 4
Case 4:	20	50	10, 8, 6, 4
Case 5:	20	40	10, 8, 6, 4
Case 6:	20	30	10, 8, 6, 4
Case 7:	20	20	10, 8, 6, 4
Case 8:	70	50	10, 8, 6, 4
Case 9:	70	40	10, 8, 6, 4
Case 10:	70	30	10, 8, 6, 4

Table 3 Criterion for Determination of Flow Reversal

Parameter Calculated	Equation For the Parameter
Mass Flow Ratio of Two Phases, X.	$\lambda = \frac{\rho u}{\rho_0 u_0}$
Potential Core Length X_p	$\frac{X_p}{d_0} = 4 + 55\lambda$
Modified Thring-Newby Parameter θ'.	$\theta' = \frac{\dot{m} + \dot{m}_0}{\dot{m}_0} \frac{d_0}{2L} \left(\frac{\rho_0}{\rho}\right)^{1/2}$
Location of Flow Reversal Initiation, X_N	$X_N = 6.25\theta' L$
*Axial Distance from Nozzle Exit to Spray Interaction with Wall, X_w.	$\frac{L}{X_w} = \frac{1}{4 + 55\lambda}$
Existence of Flow Reversal	If $X_N < X_w$
Mass Flow of Recirculation	$\frac{\dot{m}_r}{\dot{m}_0 + \dot{m}} = \frac{0.47}{\theta'} - 0.5$

where

P = Cocurrent flow n density

P_0 = water density

u = cocurrent air flow velocity

u_0 = centerline velocity at nozzle exit

d_0 = nozzle orifice diameter

m = mass flow rate of cocurrent air

m_0 = mass flow rate at nozzle exit

2L = Hydraulic diameter of the duct

* This is the distance at which the spray will impinge upon the wall due to spray spreading angle.

Table 4 Comparison of Flow Reversal Criterion with Eperimental Results

Atomizer Water Flow Rate(cc/min)	Atomizer Air Pressure (psig)	Cocurrent Air Velocity (m/s)	Predicted Flow Reversal	Experimental Flow Reversal
50	50	10	NO	NO
50	50	8	YES	YES
50	50	6	YES	YES
50	40	10	NO	NO
50	40	8	NO	NO
50	40	6	YES	YES
50	30	10	NO	NO
50	30	8	NO	NO
50	30	6	YES	YES
50	30	4	YES	YES
20	50	10	NO	NO
20	50	8	NO	NO
20	50	6	YES	YES
20	50	4	YES	YES
20	40	10	NO	NO
20	40	8	N0	NO
20	40	6	YES	YES
20	40	4	YES	YES
20	30	10	NO	NO
20	30	8	NO	NO
20	30	6	YES	YES
20	30	4	YES	YES
20	20	10	NO	NO
20	20	8	NO	NO
20	20	6	YES	YES
20	20	4	YES	YES
70	50	10	NO	NO
70	50	8	NO	NO
70	50	6	YES	YES
70	40	10	NO	NO
70	40	8	NO	NO
70	40	6	YES	YES
70	30	10	NO	NO
70	30	8	NO	NO
70	30	6	YES	YES

TABLE 5 RANGES OF NON-DIMENSIONAL PARAMETERS

NON-DIMENSIONAL PARMETERS	FORMULATION	RANGES OBTAINED DURING TESTING
Reynolds No. (duct)	$Re_D = \rho u d_h / \mu$	2.2×10^5 - 6.2×10^5
Reynolds No. (air)	$Re_a = (\dot{m} + \dot{m}_a) d_h / A_c \mu$	2.5×10^5 - 6.5×10^5
Reynolds No. (spray)	$Re_s = \rho u_m D_s / \mu$	4.0×10^2 - 4.0×10^3
Velocity Ratio	u_c/u (at x= 5cm)	5.0 - 35.0
Velocity Ratio	u_c/u (at x= 10cm)	2.5 - 22.0
Recirculation mass flow ratio	$\frac{\dot{m}r}{\dot{m}_0 + \dot{m}}$	0.12 - 0.34

APPENDIX-A

ERROR ANALYSIS

It is very important to consider the factors of error in any experimental exercise. This section briefly describes the various experimental errors encountered and where possible, a best estimate is made of their magnitude.

Error sources associated with PDA/LDA measurements

The error sources that possibly could effect the accuracy of the PDA/LDA measurements are the following:

(a) refractive index error

(b) inaccuracies in optical parameters

(a) Refractive index errors

Variations of the index of refraction of the fluid medium can cause the laser beams passing through it to follow an irregular path. The temperature and pressure dependence of the refractive index is given as;

$$n-1=7.92\times10^{-7}P/T \qquad (A1)$$

where P is the absolute pressure and T is the absolute temperature (Kadaba, (8)). In our case the refractive index error is negligible due to the relative change in the index of refraction being negligible.

(b) Inaccuracy in optical parameters

The laser wavelength, beam separation distance, beam intersection angle, and probe volume dimensions can be determined very accurately. The errors due to these inaccuracies are negligible.

Duct and Atomizer Flow

The air flow in the duct was seeded with talcum powder enabling LDA measurements for flow velocity. The range of velocity variation measured using the LDA is ±1%. Particle size accuracy is within 4% according to Dantec's PDA User's Manual.

Visual Measurements

Atomizer water flow rate and air pressure were regulated using a flow meter and pressure gauge respectively. Readings from these devices were used in several calculations. The accuracy of the water flow rate is estimated as ±5%. The pressure gauge readings are estimated at an accuracy of ±3%.

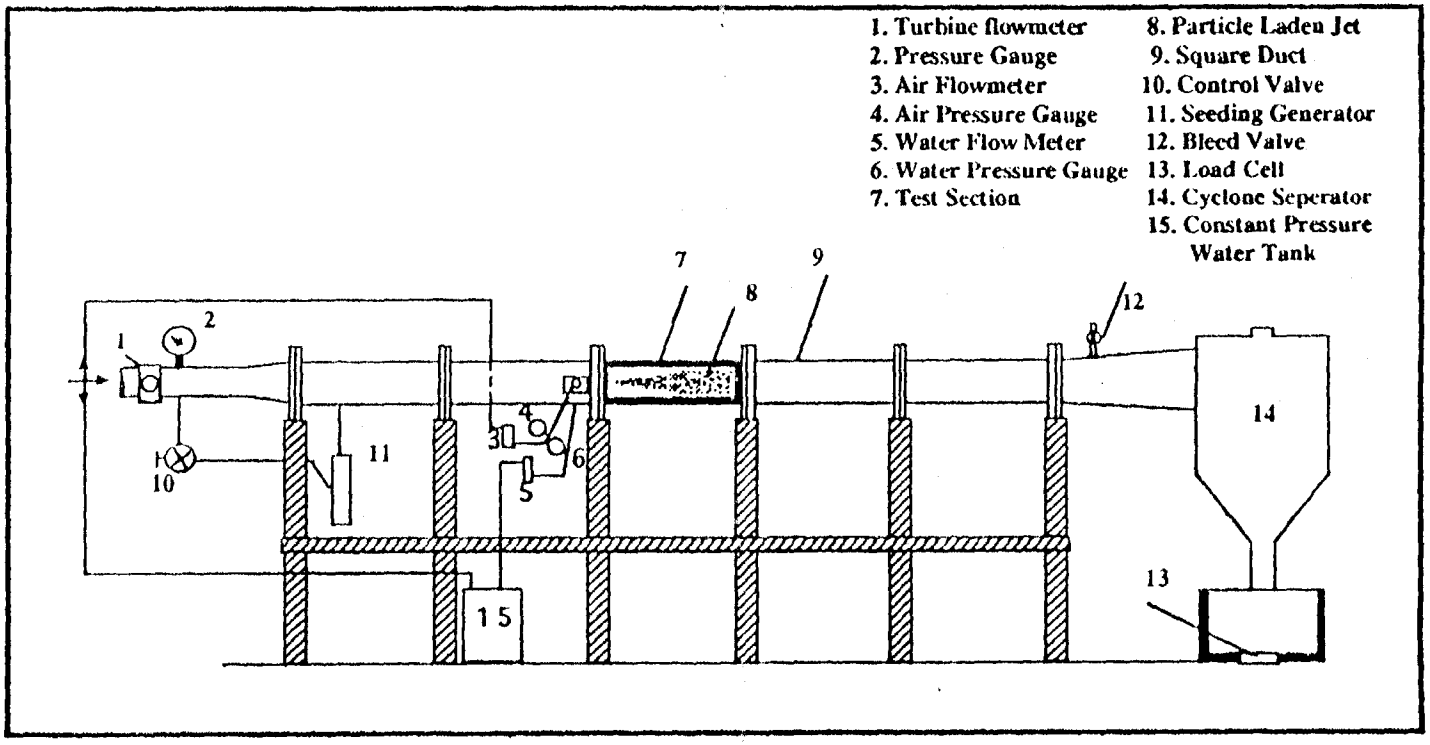

Figure 1 Schematic of Test Facility

Figure 2 Glass particle size distribution obtained from PDA and TTLDV (160mm lens), (TTLDV mean = 41.0 um, PDA mean = 43.2 um).

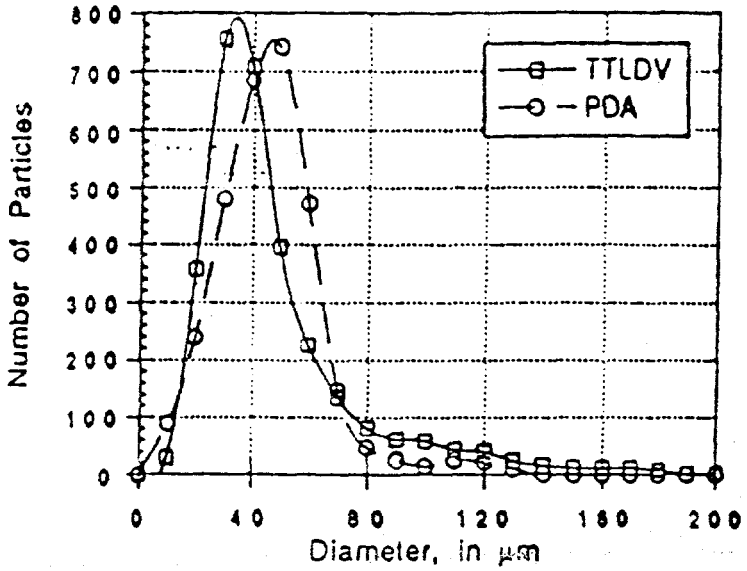

Figure 3 Comparision of lime particle size distribution obtained from TTLDV and PDA tests, and Microtrac results. (Cumulative results)

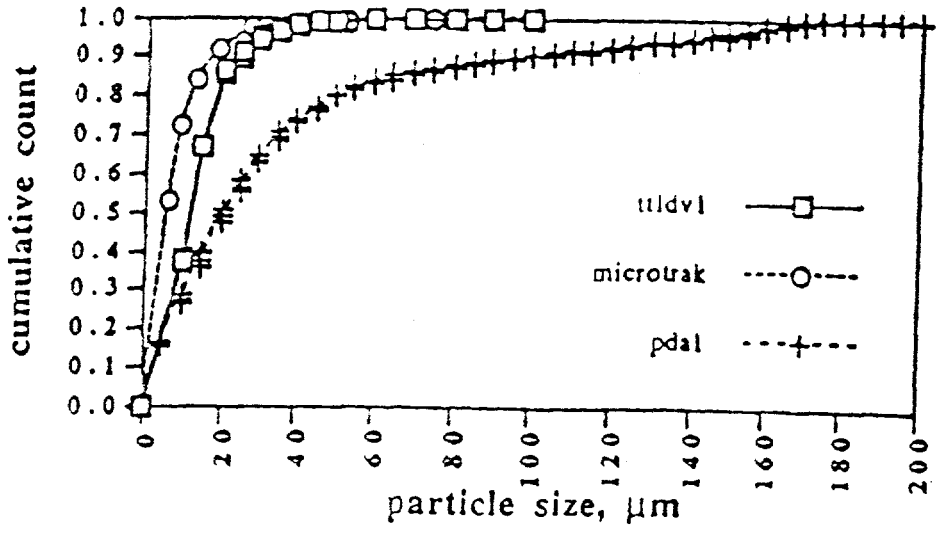

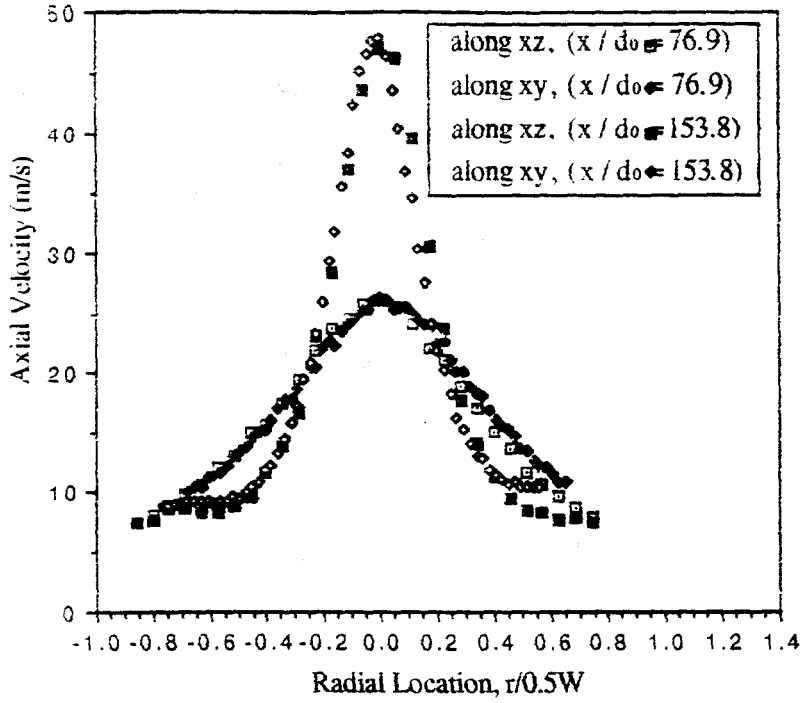

Figure 4(a) Velocity profiles showing axisymmetric spray

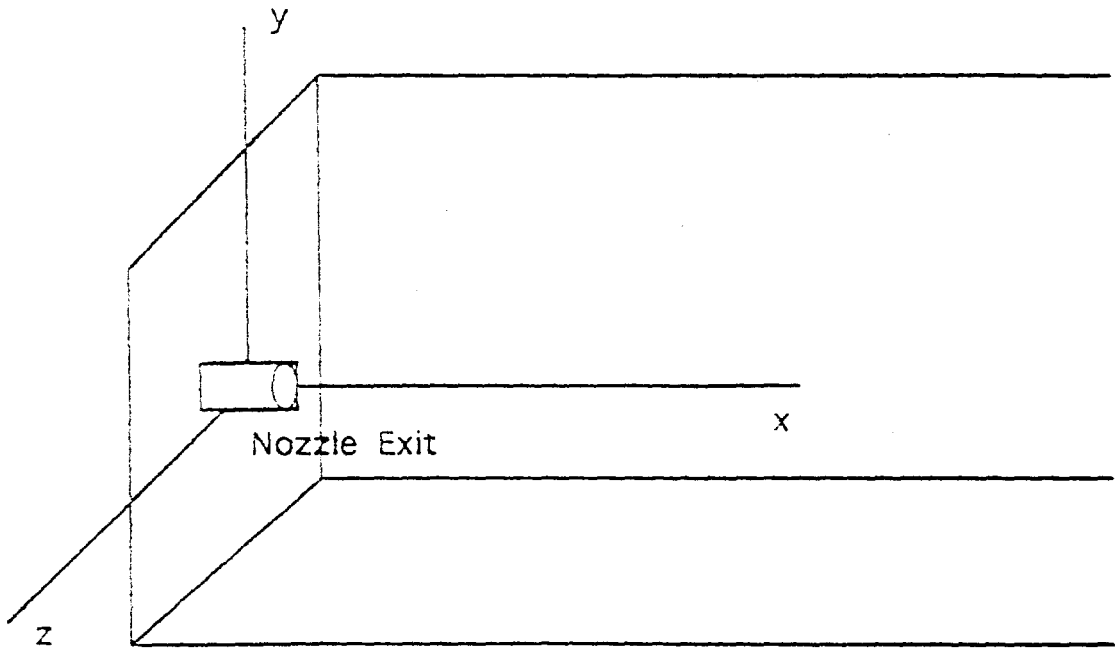

Figure 4b Spray Coordinates defining axisymmetry

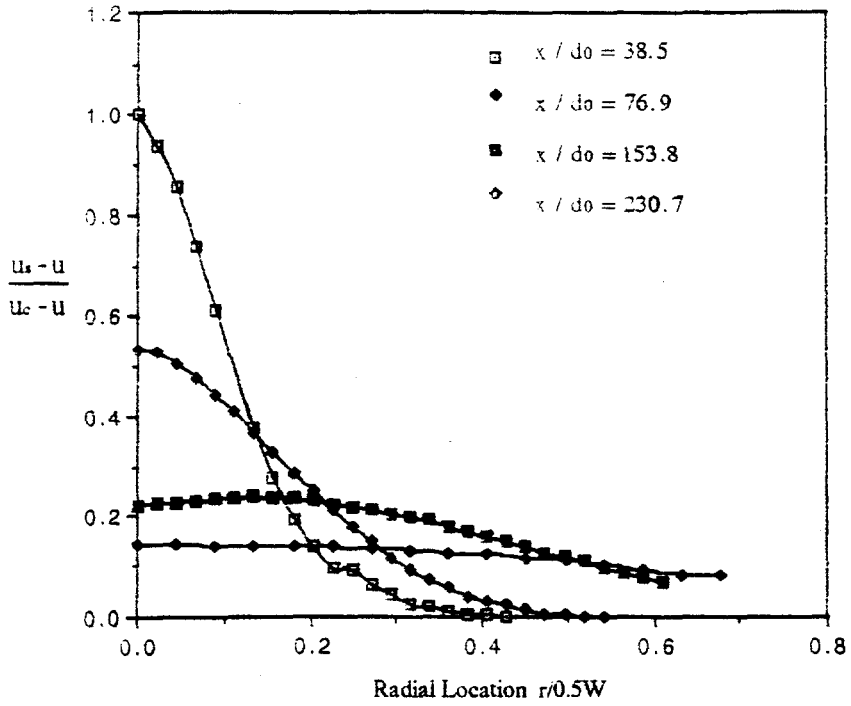

Figure 5 Velocity Profiles at the four total measurement planes for Case 1; Uo=684.94 m/s, U= 10 m/s

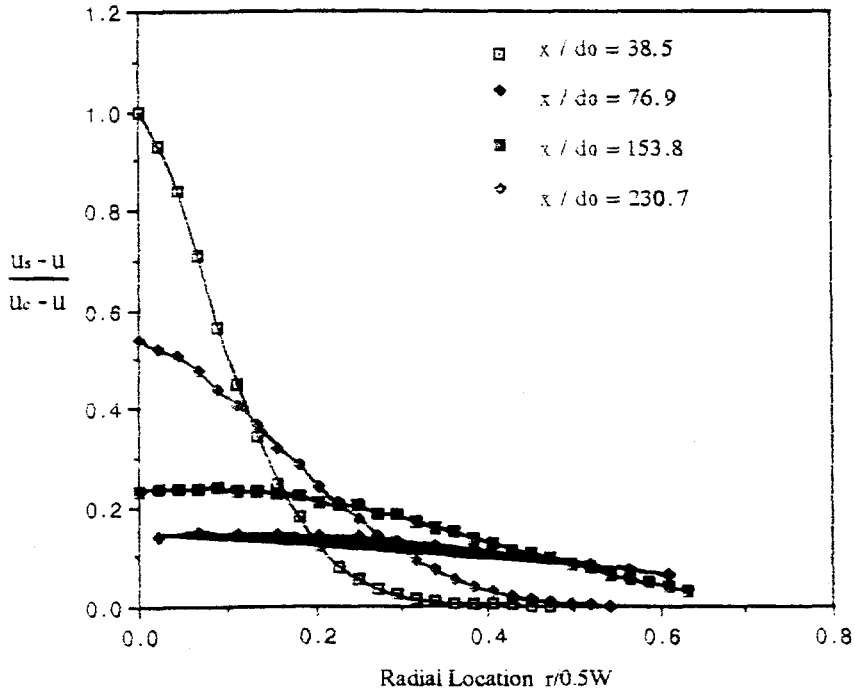

Figure 6 Velocity profiles at the four axial measurement planes for case 2; Uo= 573.05 m/s, U= 10 m/s

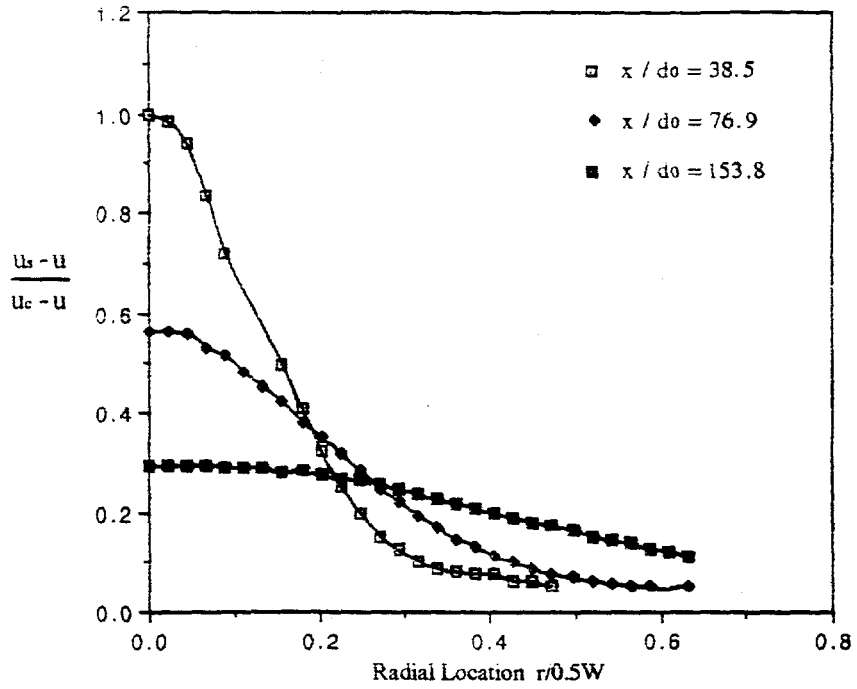

Figure 7 Velocity profiles at the four axial measurement planes for Case 2: u0=573.05m/s, u=6m/s

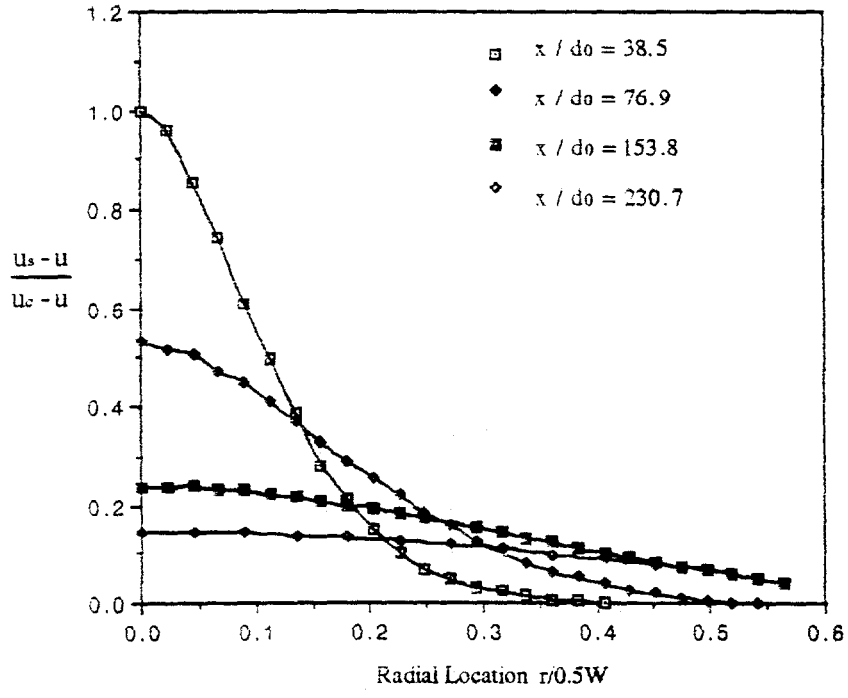

Figure 8 Velocity profiles at the four axial measurement planes for Case 3: u0=466.45m/s, u=8m/s

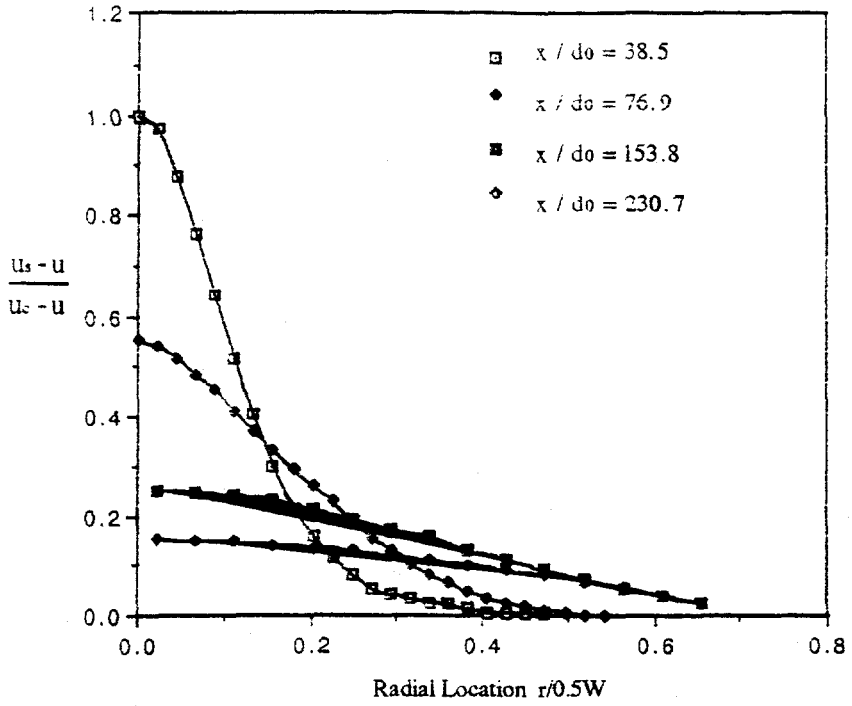

Figure 9 Velocity profiles at the four axial measurement planes for Case 4: u_0=681.48m/s, u=10m/s

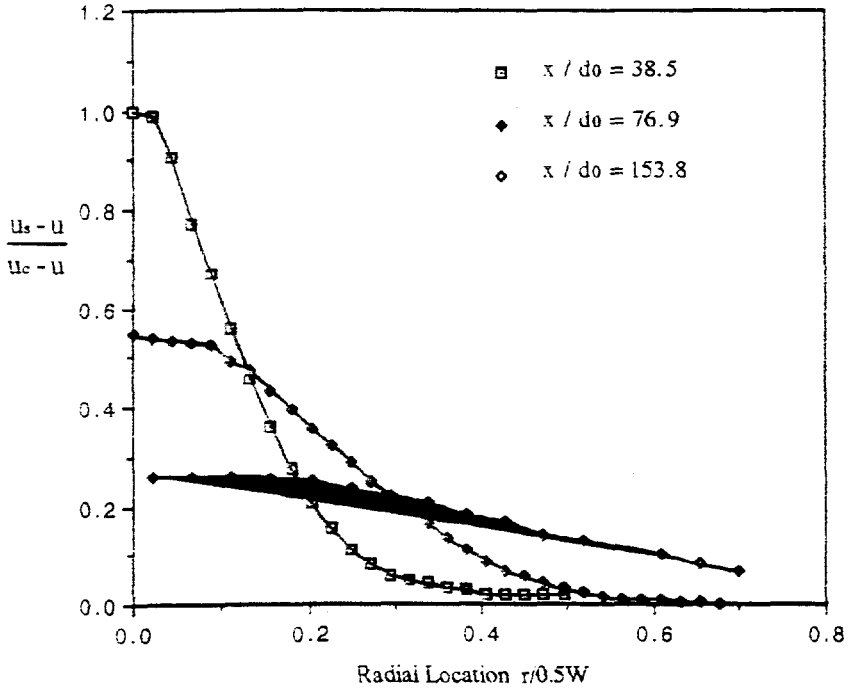

Figure 10 Velocity profiles at the three axial measurement planes

for Case 5: u_0= 571.36m/s, u=8m/s

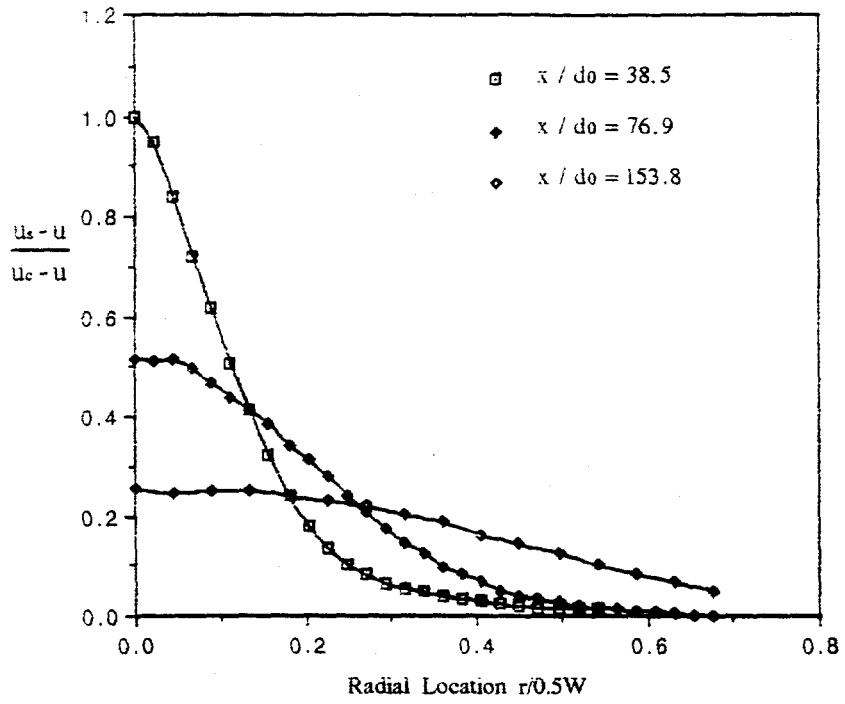

Figure 11 Velocity profiles at the three axial measurement planes for Case 6: u0=465.26m/s, u=4m/s

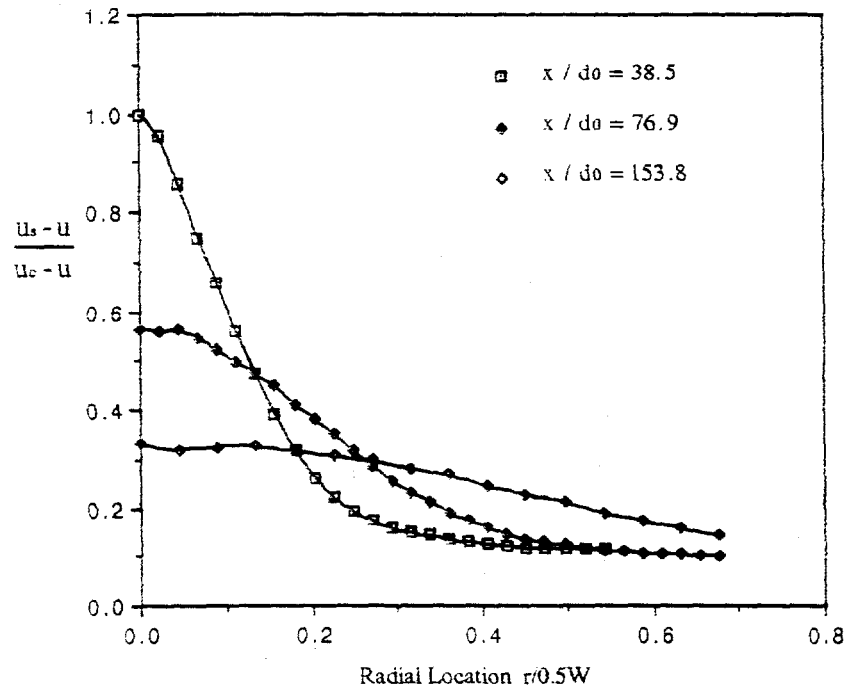

Figure 12 Velocity profiles at the three axial measurement planes for Case 8: u0=682.76m/s, u=10m/s

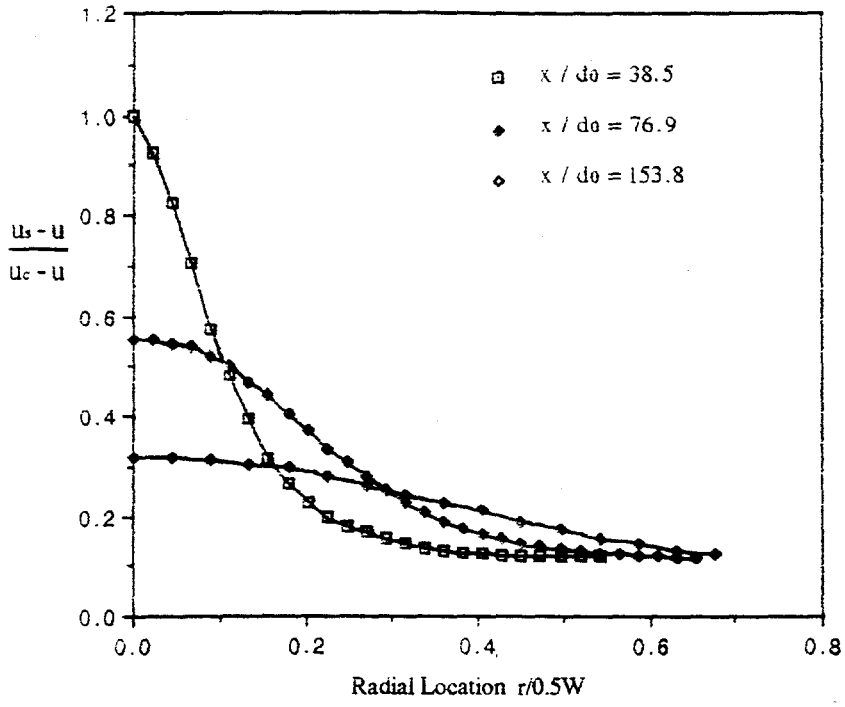

Figure 13 Velocity profiles at the three axial measurement planes for Case 9: u0=573.60m/s, u=10m/s

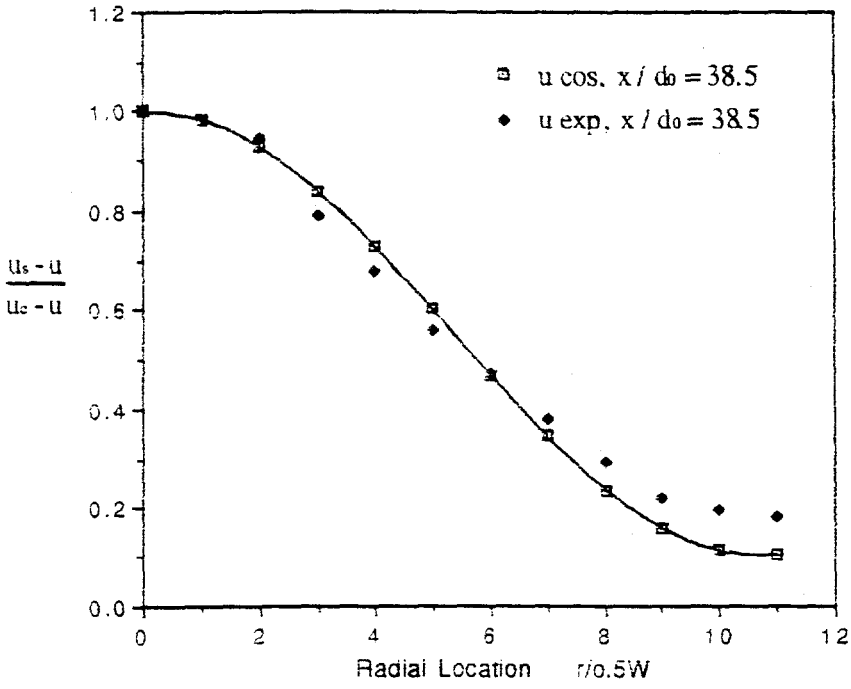

Figure 14 Comparison of experimental velocity profile with cosine model for Case 4: u0=681.48m/s, u=10m/s

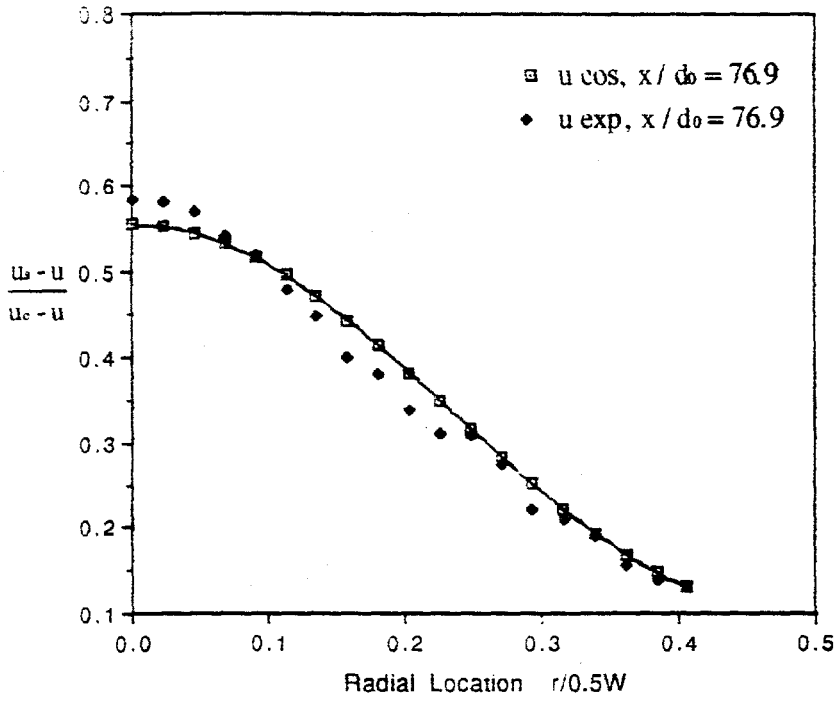

Figure 15 Comparison of experimental velocity profile with cosine model for Case 4: u0=681.48m/s, u=8m/s

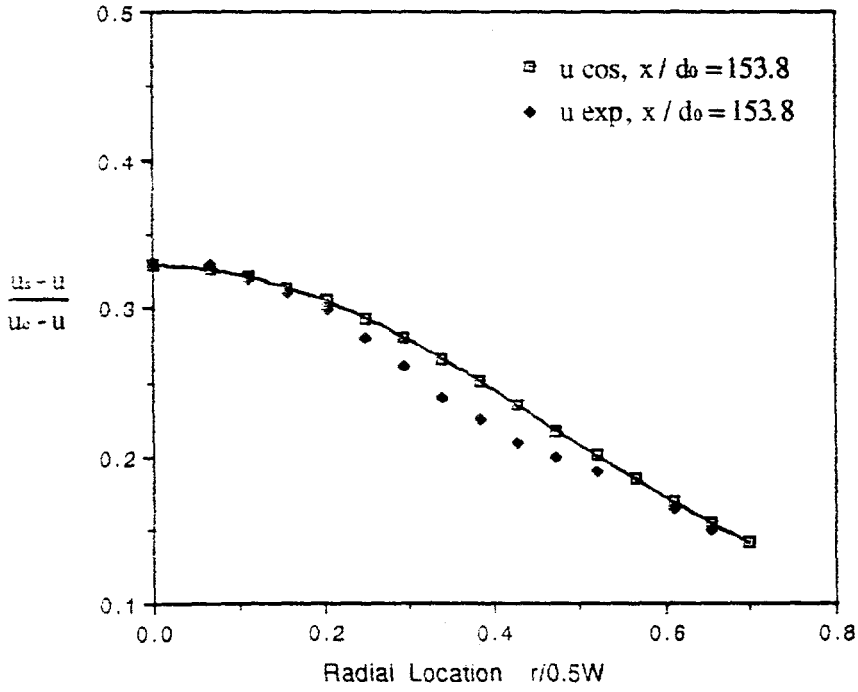

Figure 16 Comparison of experimental velocity profile with cosine model for Case 4: u0=681.48m/s, u=6m/s

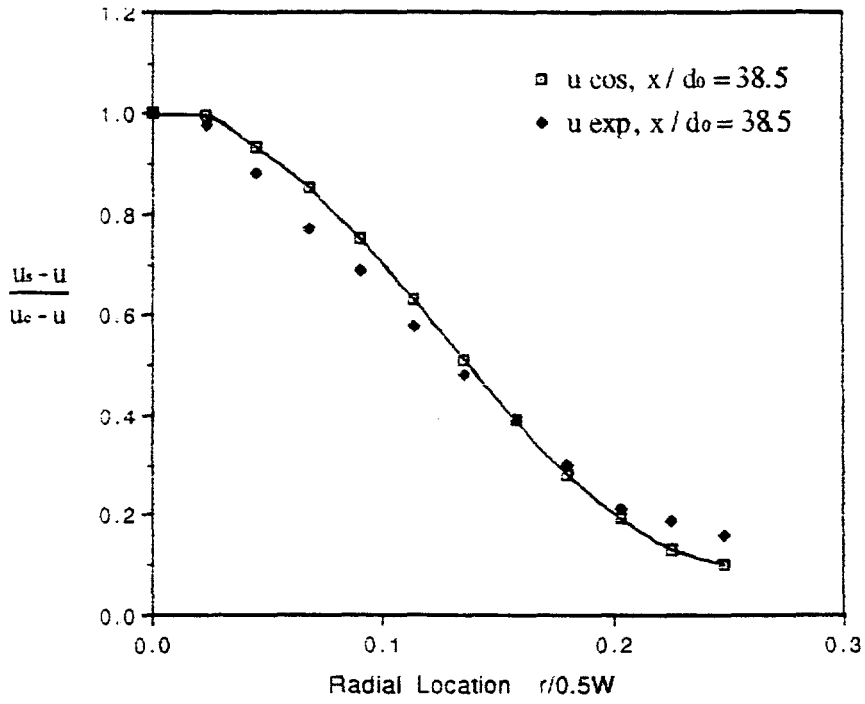

Figure 17 Comparison of experimental velocity profile with cosine model for Case 8: u0=682.76m/s, u=10m/s

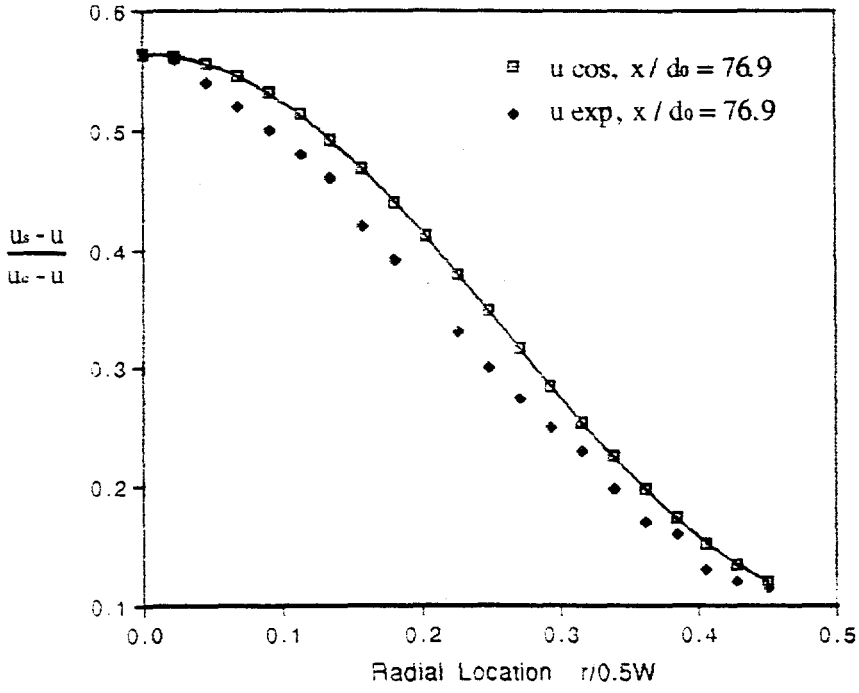

Figure 18 Comparison of experimental velocity profile with cosine model for Case 8: u0=682.76m/s, u=8m/s

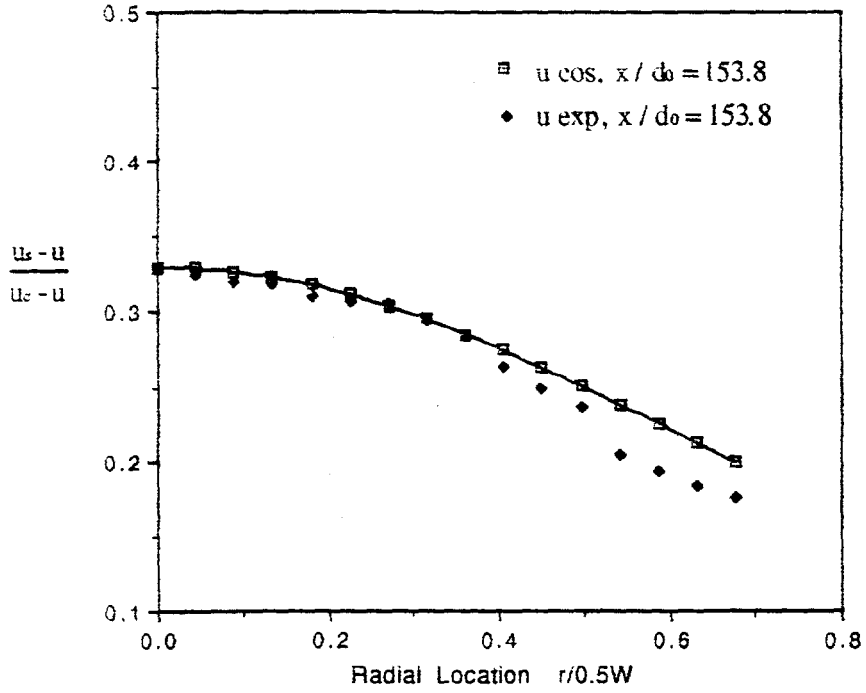

Figure 19 Comparison of experimental velocity profile with cosine model for Case 8: u0=682.76m/s, u=6m/s

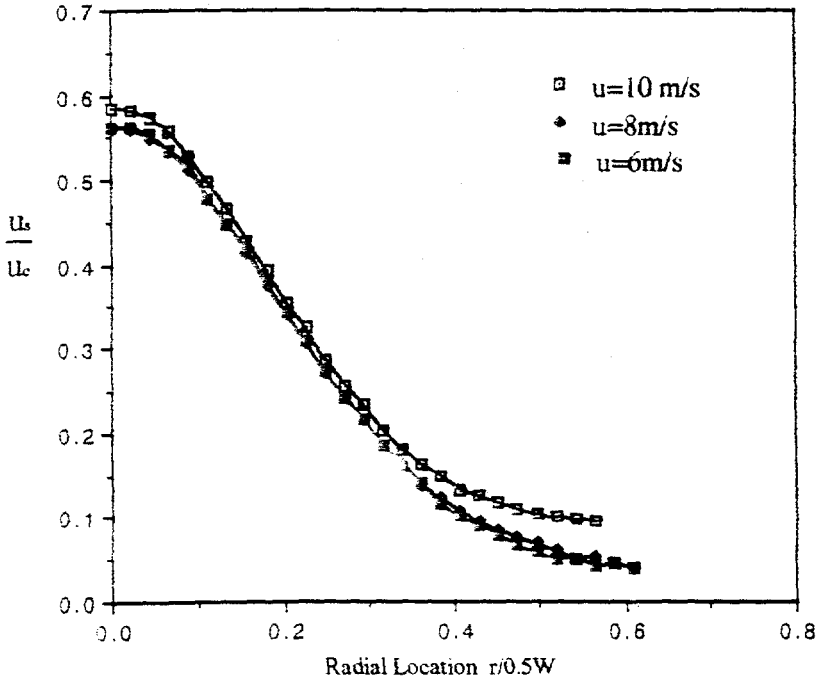

Figure 20 Velocity profiles for Case 1(u0=684.94m/s) at the x/d0=76.9 measurement plane for three cocurrent velocities

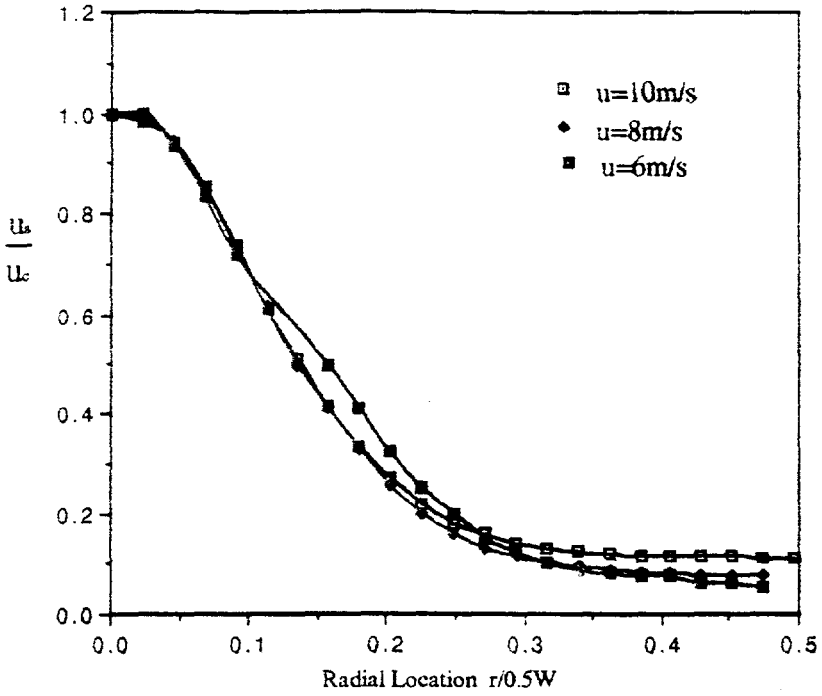

Figure 21 Velocity profiles for Case 2(u_0=573.05m/s) at the x/d_0=38.5 measurement plane for three cocurrent velocities

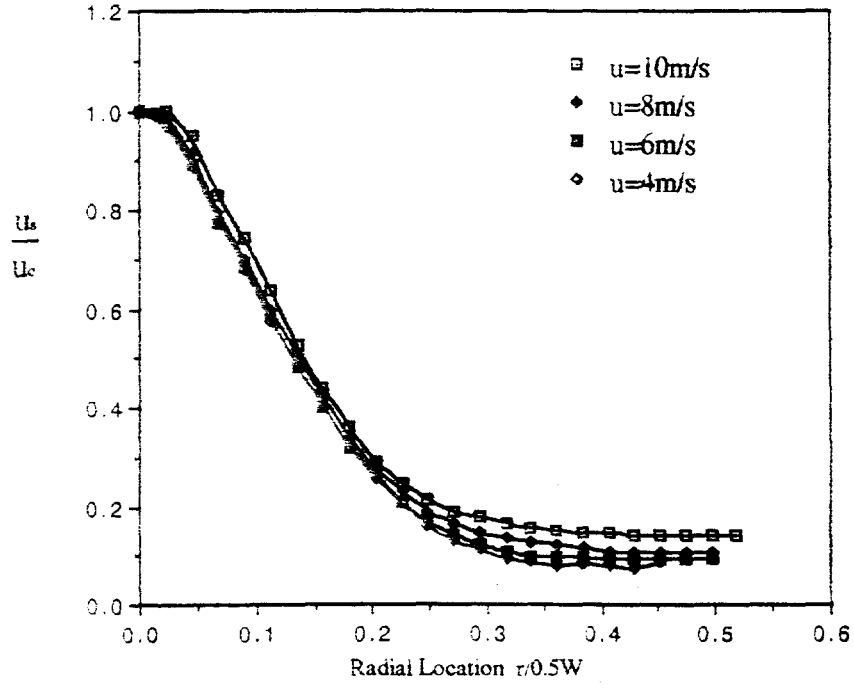

Figure 22 Velocity profiles for Case 5(u_0=571.36m/s) at the x/d_0=38.5 measurement plane for four cocurrent velocities

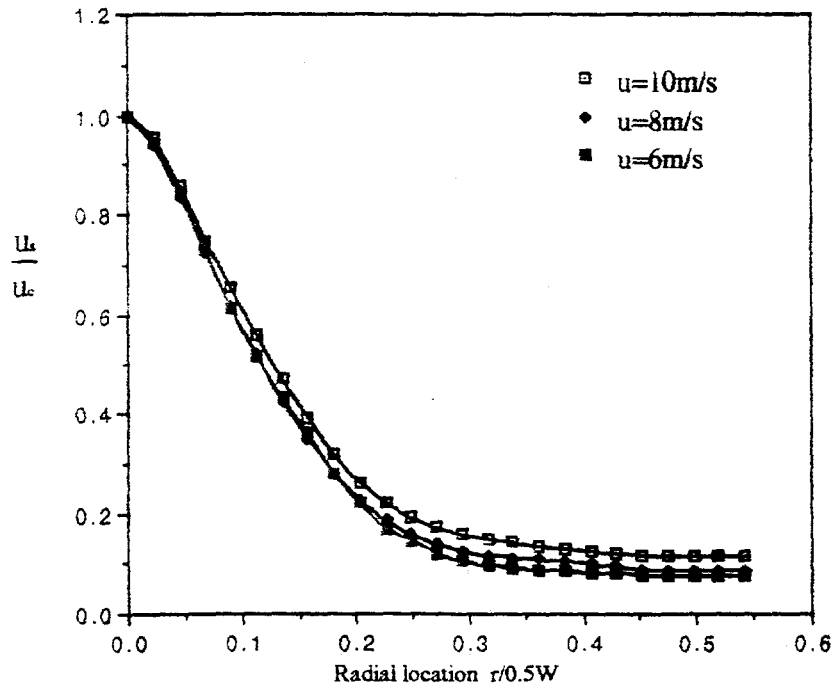

Figure 23 Velocity profiles for Case 8(u_0=682.76m/s at the x/d_0=38.5 measurement plane for four cocurrent velocities

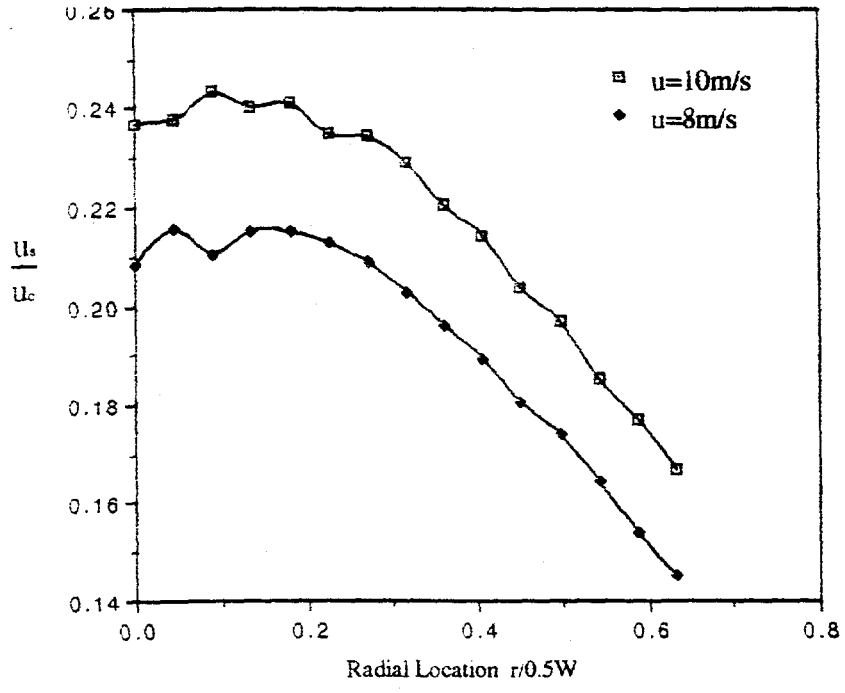

Figure 24 Velocity profiles for Case 3(u_0=466.45m/s) at the x/d_0=230.7 measurement plane for two cocurrent velocities

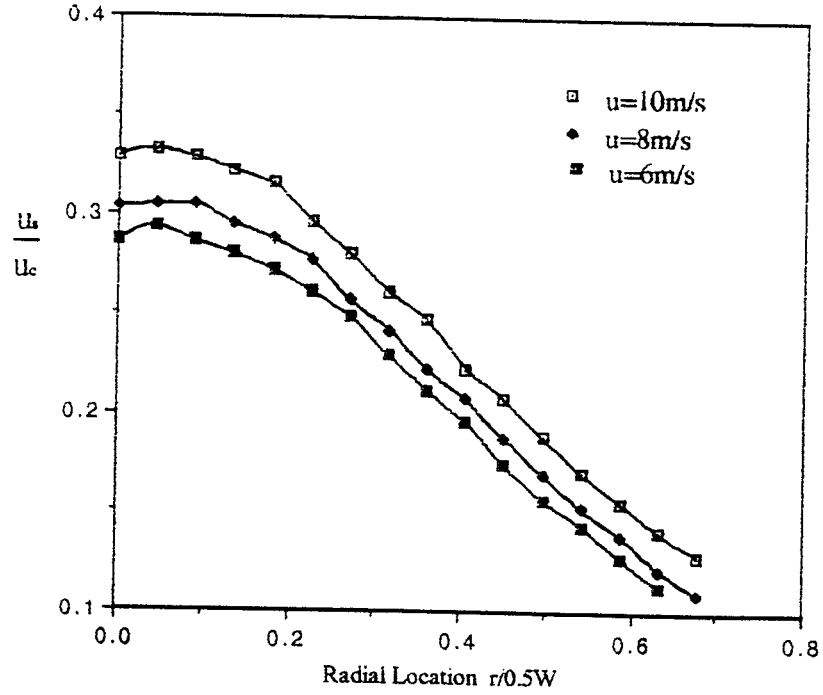

Figure 25 Velocity profiles for Case 4(u0=681.48 m/s) at the x/d0=153.8 measurement plane for three cocurrent velocities

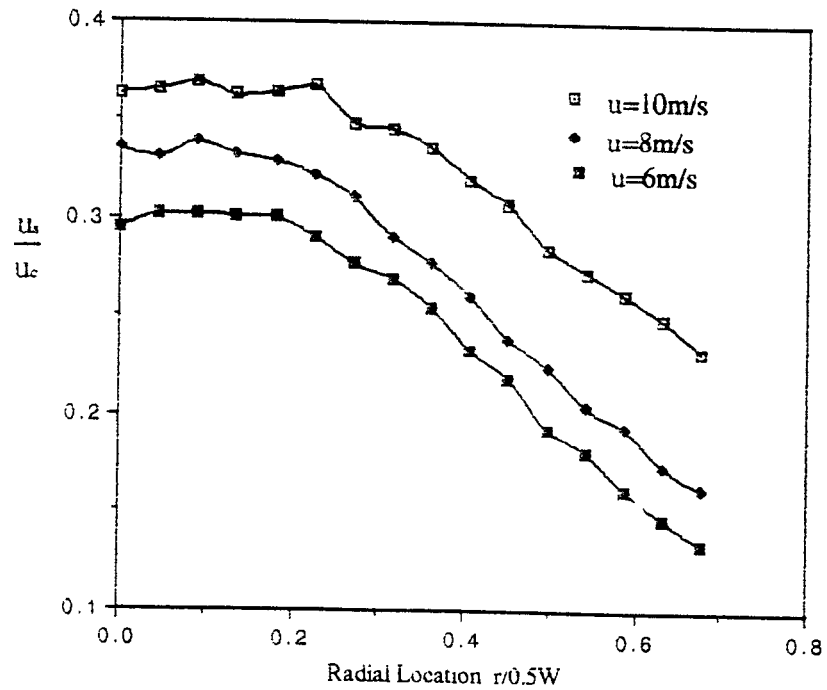

Figure 26 Velocity profiles for Case 7(u0=427.73m/s) at the x/d0=153.8 measurement plane for three cocurrent velocities

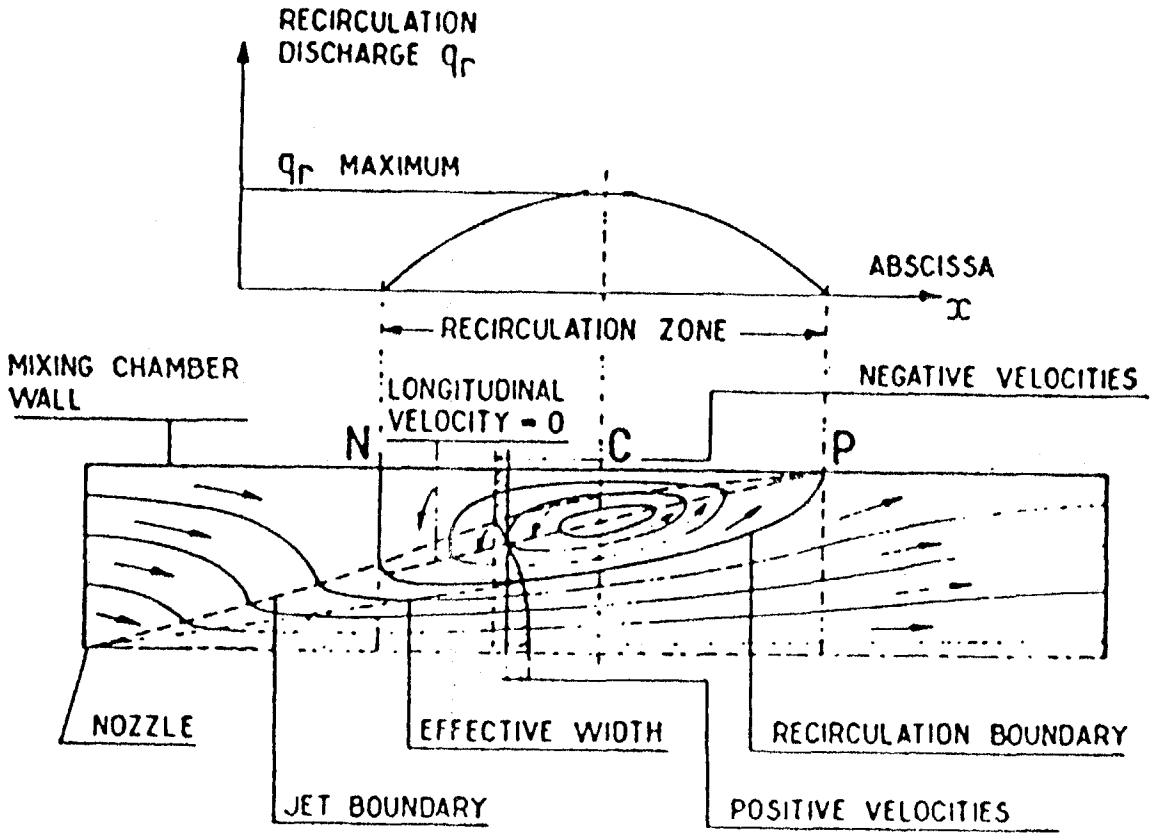

Figure 27 Map of flow field showing flow reversal[Reference]

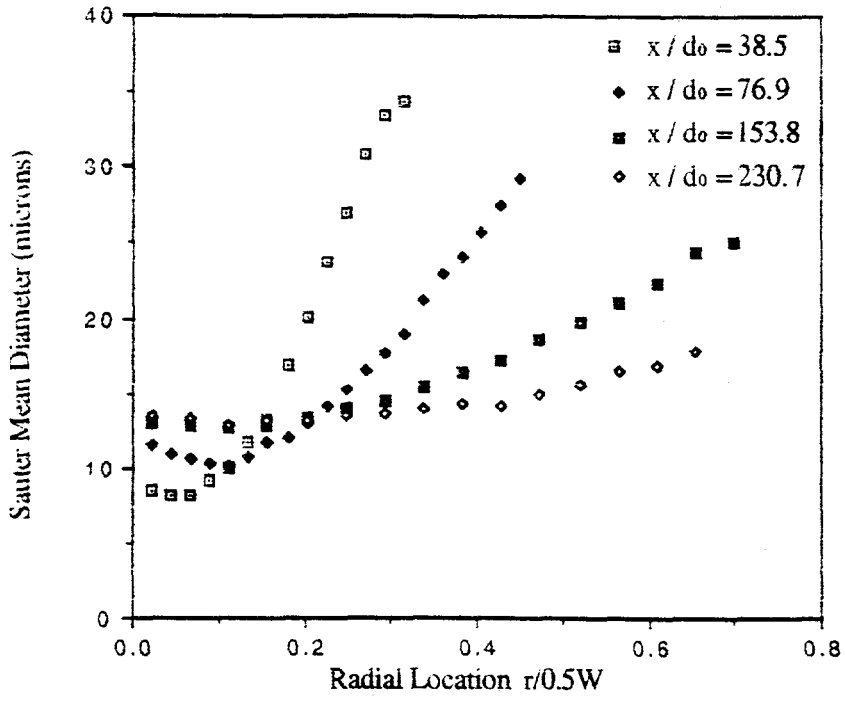

Figure 28 Particle size distribution for Case 4: u0=681.48m/s, u=10m/s

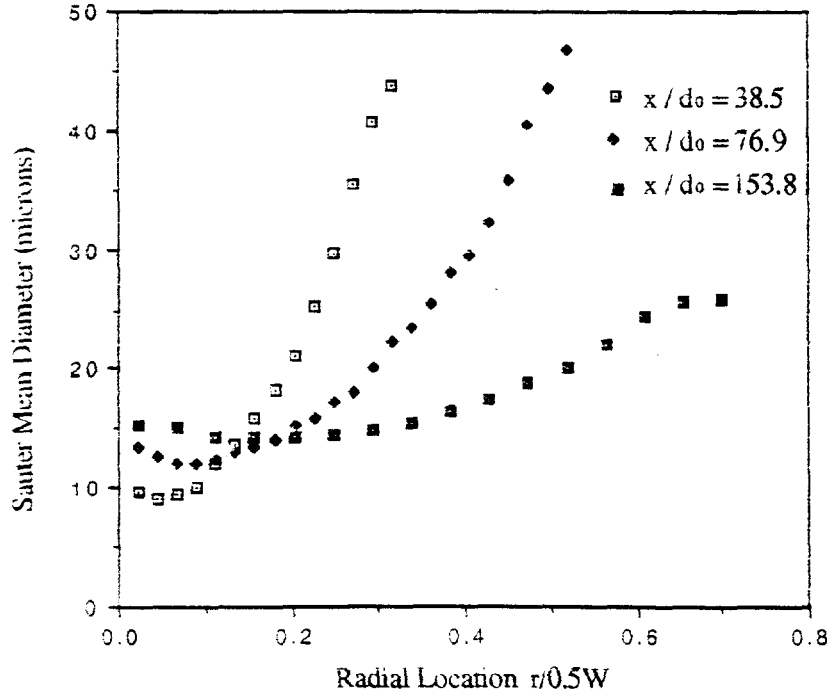

Figure 29 Particle size distribution for Case 5: u0=571.36m/s, u=6m/s

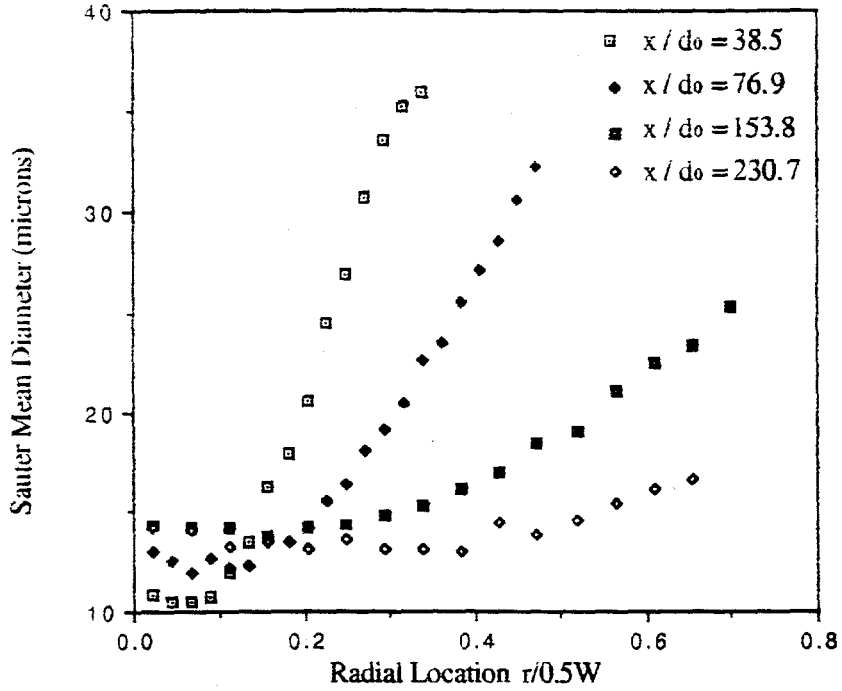

Figure 30 Particle size distribution for Case 6:. u0=465.26m/s, u=8m/s

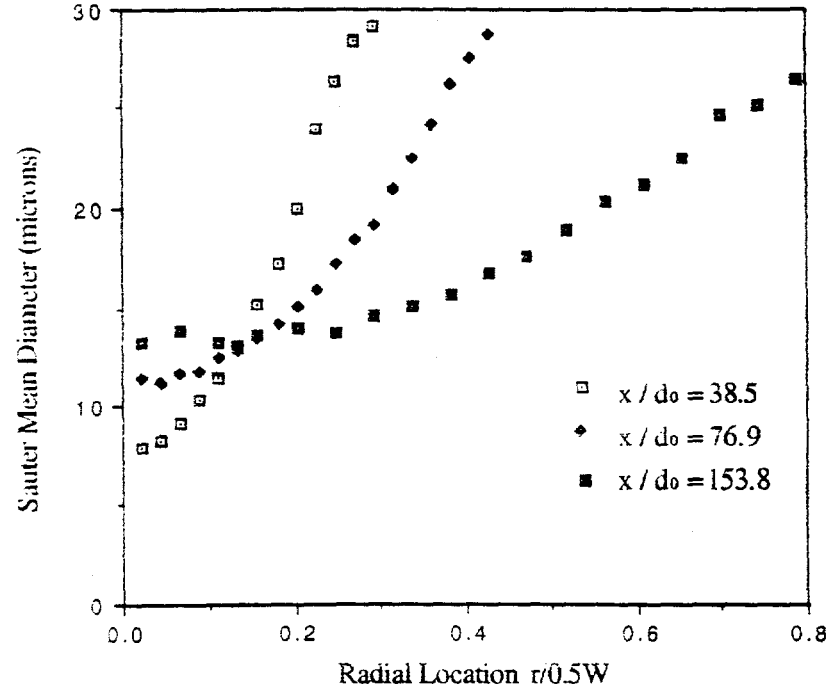

Figure 31 Particle size distribution for Case 8:; u0=682.76m/s, u=10m/s

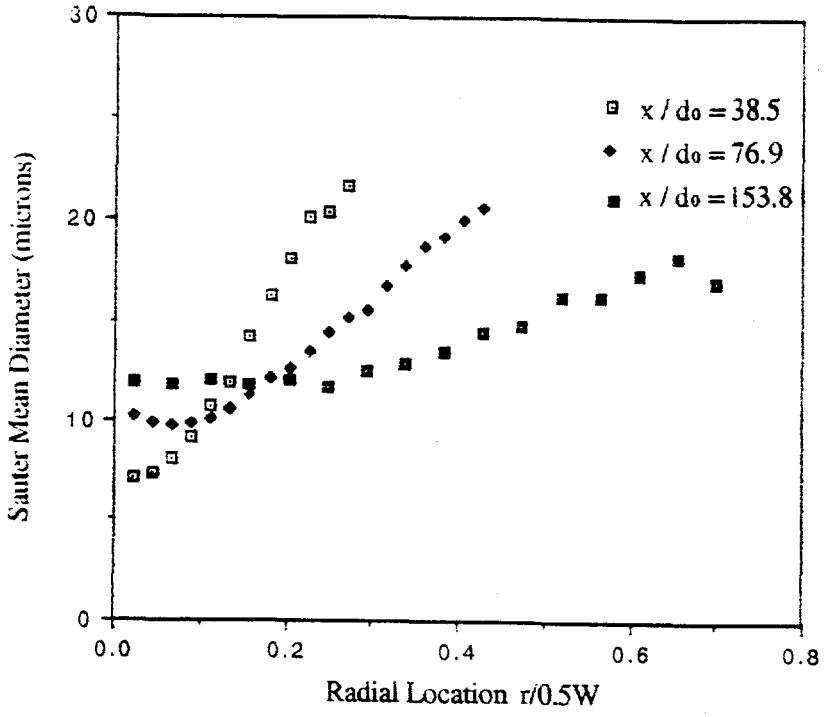

Figure 32 Particle size distribution for Case 10:: u_0=466.48m/s, u=8m/s

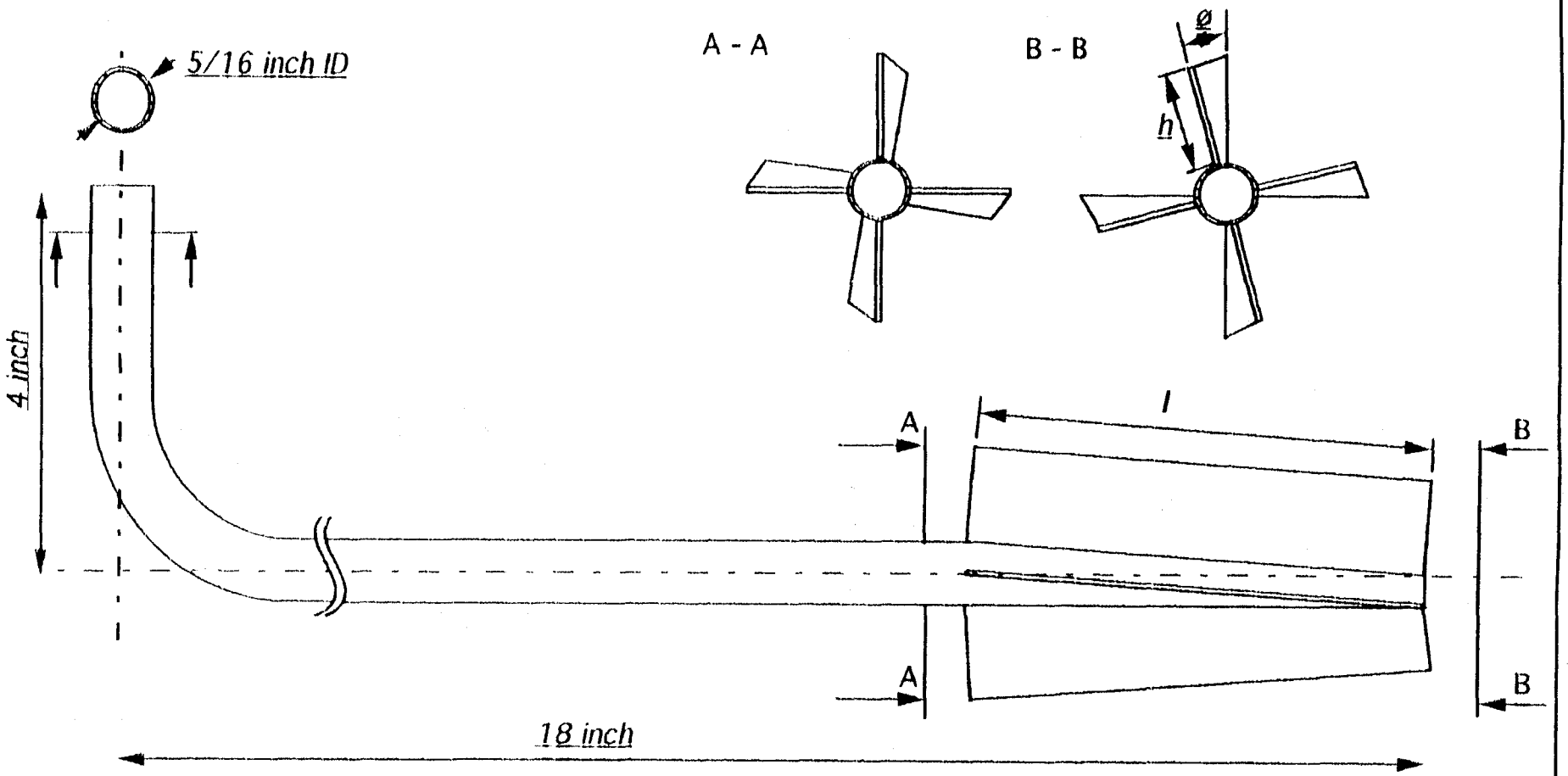

Additional design parameters

l = 10 cm and h = 1 cm
Ø = 15° and 30°

OCDO _ FLUE GAS DESULFRIZATION PROCESS
SWIRLING NOZZLE DESIGN
Ø Blade Swirl Angle and h blade height *l Blade length*

Figure 33 The Swirling Nozzle

Figure 34 The swirling nozzle set up in the test facility.

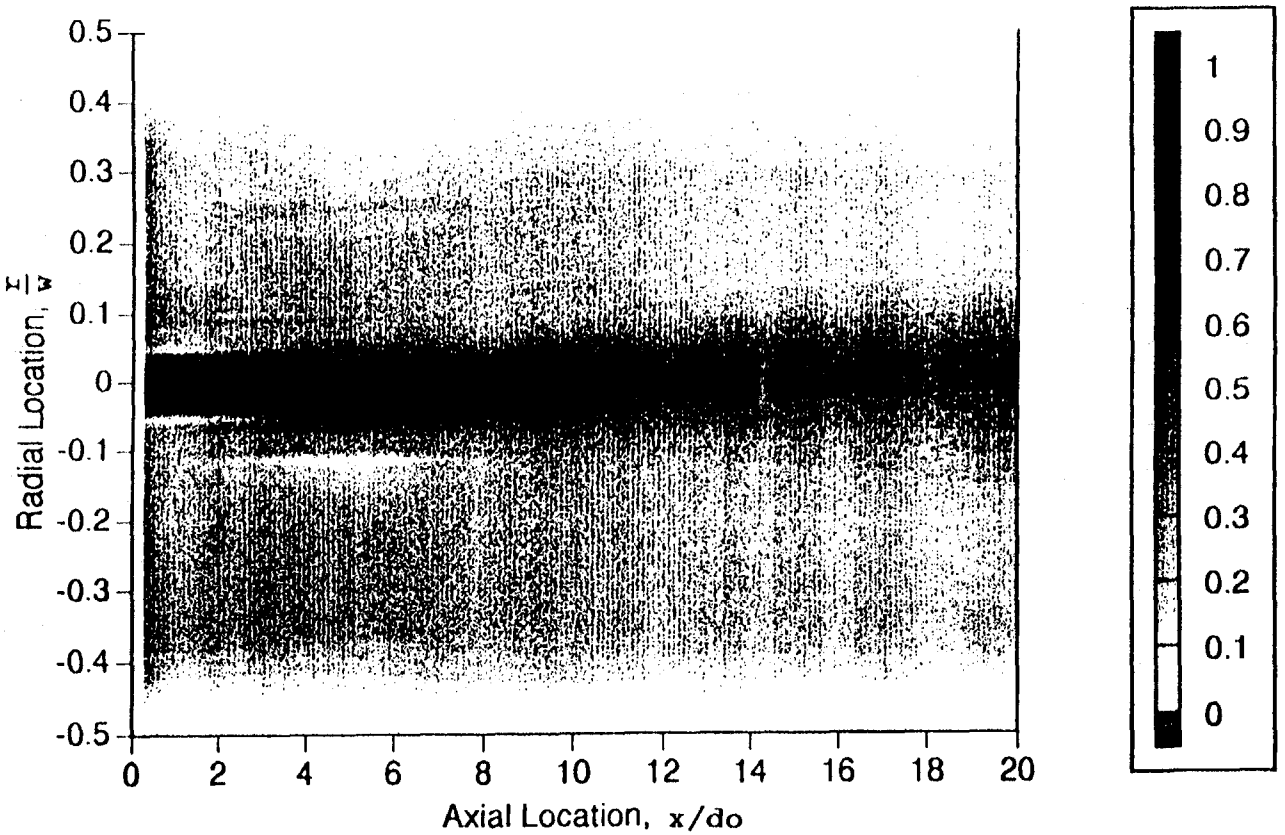

Figure 35. Velocity distribution along the axial length of the test section for swirling nozzle configuration (Cocurrent velocity = 10m/s, centerline jet velocity at nozzle exit=30m/s)

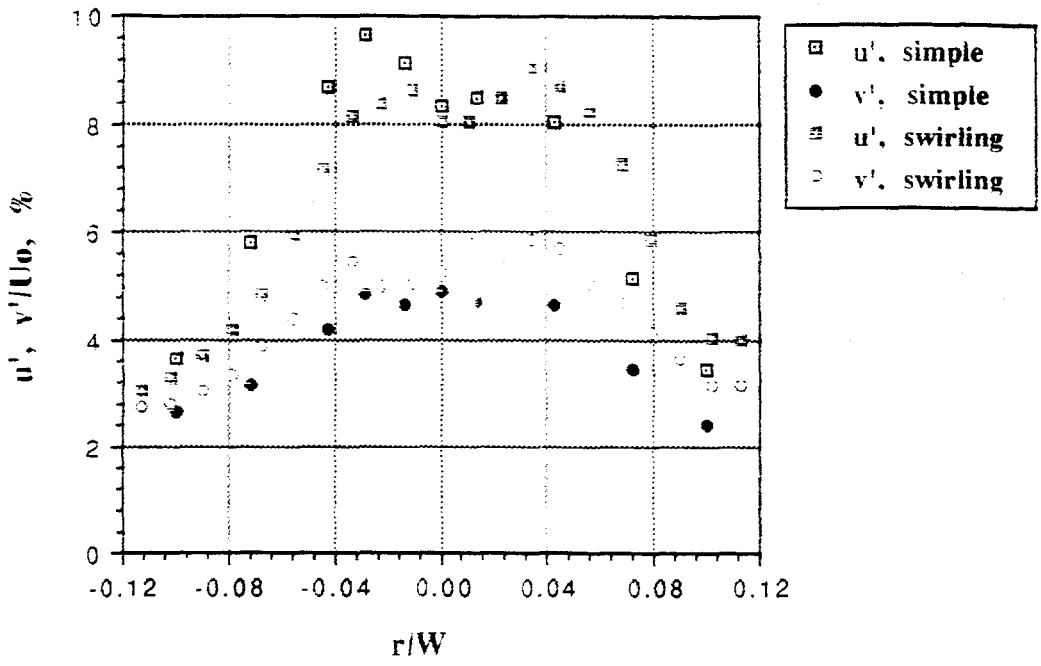

Figure 36 Comparison of axial and radial turbulent velocity data for swirling and simple nozzle. Test conditions: Jet velocity Uo= 30 m/s. cocurrent flow velocity Ud= 15 m/s, Axial location x/d= 10.

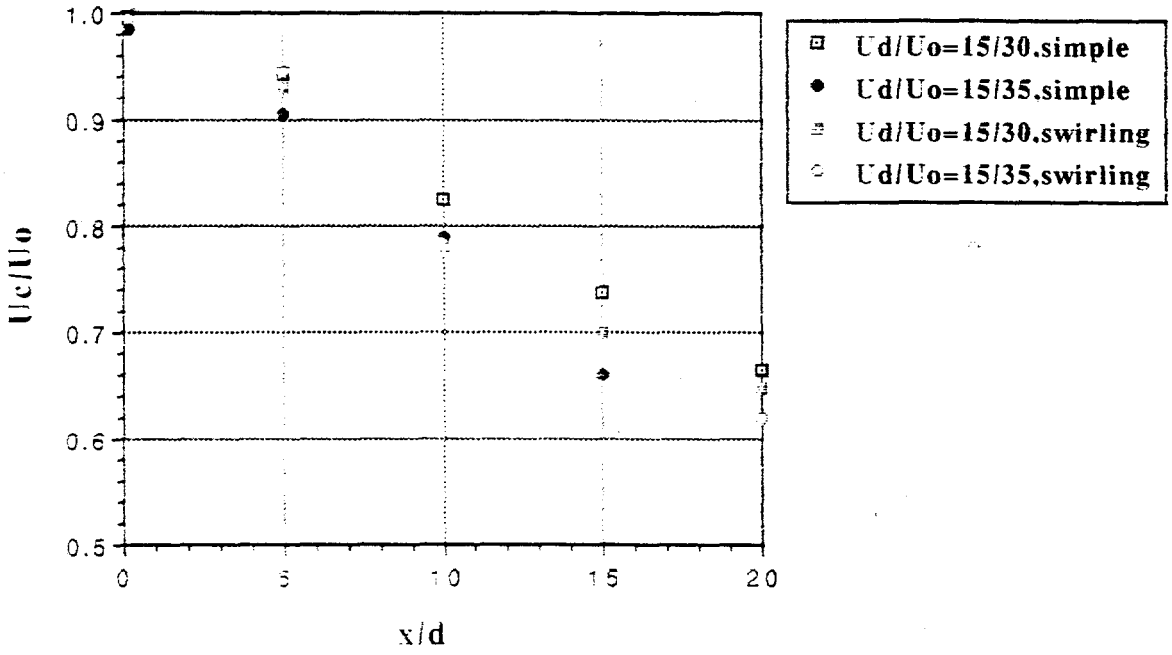

Figure 37 Decay of Jet centerline Velocity for simple and swirling nozzle configurations. Ud = duct velocity, Uo = jet velocity, Uc = Jet centerline velocity.

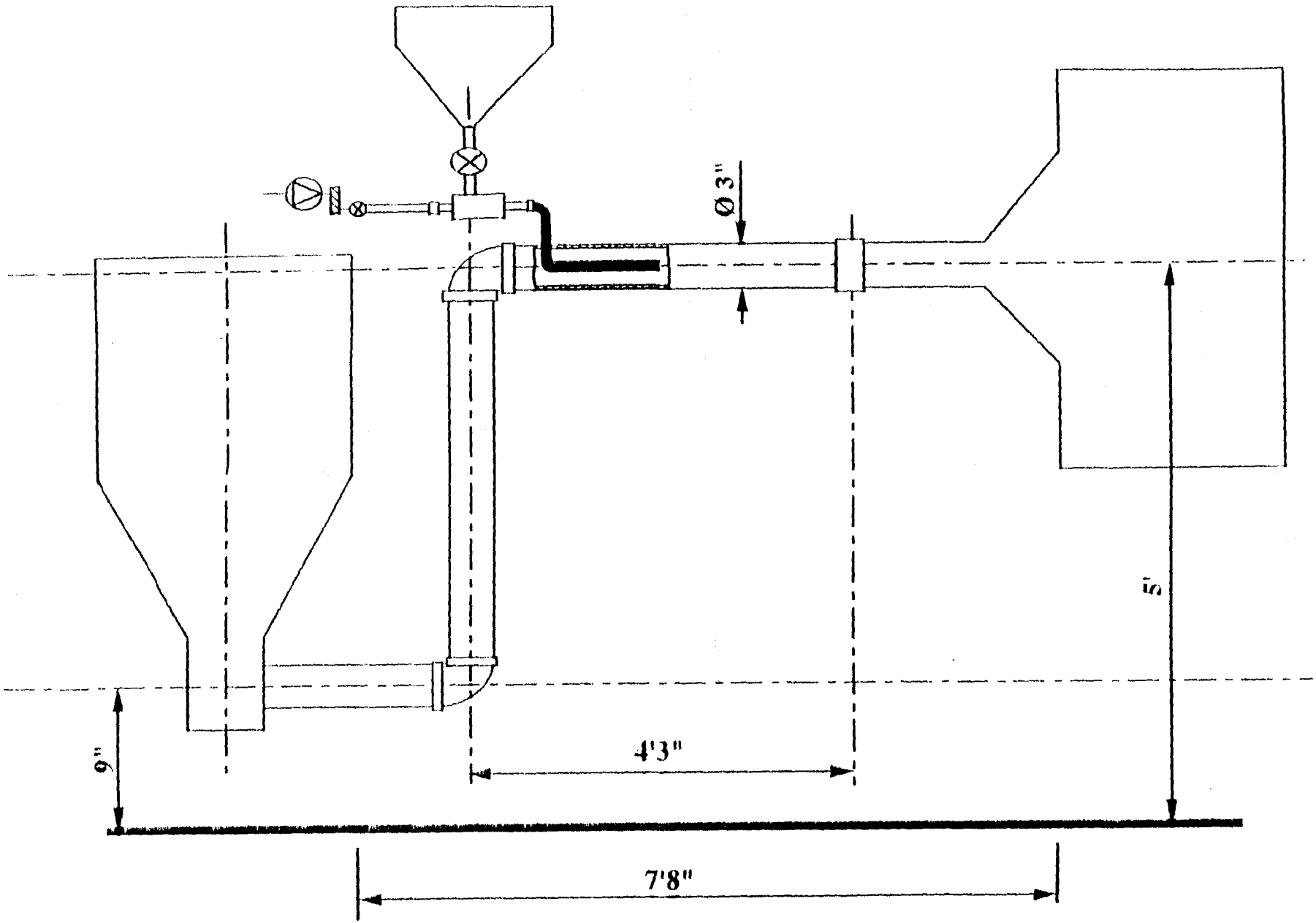

Figure 38 Simple arrangement for straight and swirling nozzle sulfur dioxide tests in University of Cincinnati's Sprayer Dryer Facility.